3-23-2017

Total electron count variability and stratospheric ozone effects on solar backscatter and LWIR emissions

John S. Ross

TOTAL ELECTRON COUNT VARIABILITY AND STRATOSPHERIC OZONE EFFECTS ON SOLAR BACKSCATTER AND LWIR EMISSIONS

THESIS

John S. Ross, Captain, USAF

AFIT-ENP-MS-17-M-103

DEPARTMENT OF THE AIR FORCE
AIR UNIVERSITY

AIR FORCE INSTITUTE OF TECHNOLOGY

Wright-Patterson Air Force Base, Ohio

AFIT-ENP-MS-17-M-103

TOTAL ELECTRON COUNT VARIABILITY AND STRATOSPHERIC OZONE EFFECTS ON SOLAR BACKSCATTER AND LWIR EMISSIONS

THESIS

Presented to the Faculty

Department of Engineering Physics

Graduate School of Engineering and Management

Air Force Institute of Technology

Air University

Air Education and Training Command

In Partial Fulfillment of the Requirements for the

Degree of Master of Science in Applied Physics

John S. Ross, BS

Captain, USAF

March 2017

AFIT-ENP-MS-17-M-103

TOTAL ELECTRON COUNT VARIABILITY AND STRATOSPHERIC OZONE EFFECTS ON SOLAR BACKSCATTER AND LWIR EMISSIONS

John S. Ross, BS
Captain, USAF

Committee Membership:

Dr. S. T. Fiorino
Chair

Dr. R. D. Loper
Member

Lt Col R. A. Stenger
Member

Abstract

The development of an accurate ionospheric Total Electron Content (TEC) model is of critical importance to High Frequency (HF) radio wave propagation. However, the TEC is highly variable and is continuously influenced by geomagnetic storms, extreme Ultraviolet (UV) radiation, diurnal variation, and planetary waves. The ability to capture this variability is essential to improve current TEC models. Analysis of the growing body of data involving ionospheric fluctuations and thermal tides has revealed persistent correlation between increases in stratospheric ozone and variability of the TEC. The spectral properties of ozone show that it is a greenhouse gas that alters longwave emissions from Earth and interacts with the UV spectrum coming from the sun. This study uses the Laser Environment Effects Definition and Reference (LEEDR) to model and simulate the effect of changes in stratospheric ozone on solar backscatter and longwave terrestrial emissions and infer TEC variability.

Table of Contents

Page

List of Figures

Page

List of Tables

Page

List of Acronyms

AIRS - Atmospheric Infrared Sounder

BUV - Backscatter UltraViolet

CAWSES II - Climate and Weather of the Sun-Earth System

CORS - Continually Operating Reference Station

EOS - Earth Observing System

EPN - EUREF Permanent Network

ExPERT - Extreme and Percentile Environmental Reverence Tables

GADS - Global Aerosol Data Set

GAIM - Global Assimilation of Ionospheric Measurements

GIM - Global Ionospheric Map

GLONASS - Global Navigation Satellite System

GNSS - Global Navigation Satellite Systems

GPS - Global Positioning System

HF - High Frequency

HITRAN - High Resolution Transmission

ICON - Ionospheric Connection Explorer

IGS - International GPS Service for Geodynamics

IONEX - IONosphere Map Exchange Format

IONS-06 - INTEX Ozonesonde Network Study

IR – Infrared

IRI - International Reference Ionosphere

JPL - Jet Propulsion Laboratory

LEEDR - Laser Environment Effects Definition and Reference

LIDAR - LIght Detection And Ranging

LWIR - Longwave and Infrared

MKIV – Mark IV

MODTRAN - Moderate Resolution Transmittance

NEUBREW - NOAA-EPA Brewer Spectrophotometer UV and Ozone Network

NGS - National Geodetic Survey

NOMADS - NOAA National Operational Model Archive and Distribution System

OMI - Ozone Monitoring Instrument

OOB - Out of Band

Reg-Est - Regularized Estimation of TEC

RINEX - Receiver Independent Exchange Format

SBUV - Solar Backscatter Ultraviolet

SABER - Sounding of the Atmosphere using Broadband Emission Radiometry (SABER)

SCOTEP - Scientific Committee on Solar-Terestrial Physics (SCOTEP)

SSI - Solar Spectral Irradiance (SSI)

SSW - Sudden Stratospheric Warming

STEC - Slant TEC

SZA - solar zenith angle

TEC - Total Electron Content

TIMED - Thermosphere Ionosphere Mesosphere Energetics Dynamics

TIEGCM - thermosphere-ionosphere-electrodynamic general circulation model

TOMS - Total Ozone Mapping Spectrometer

UV - Ultraviolet

VTEC - Vertical TEC

TOTAL ELECTRON COUNT VARIABILITY AND STRATOSPHERIC OZONE EFFECTS ON SOLAR BACKSCATTER AND LWIR EMISSIONS

I. Introduction

1.1 Overview

Accurately modeling the TEC is a complex problem due to its high variability. The primary sources of daily variations in the ionosphere are fundamentally understood drivers such as the solar ionizing flux and geomagnetic activity. However, these drivers do not account for roughly 20% of F-region electron density during the day and 33% during the night (Gonsharenko et al., 2010). These ionospheric variations can be far more dramatic during periods of solar minimum and at lower latitudes. One of the other factors that has been evidenced to cause ionospheric impacts are planetary tides, which are related to stratospheric ozone densities. Fluctuations in stratospheric ozone generate the planetary tide as a result of thermal waves (Gonsharenko et al., 2012). Stratospheric ozone can be monitored with radiative and scattering/absorbing effects of UV and down-welling longwave infrared (LWIR) emissions, which in turn indicates TEC variability. Thus, changes in the UV backscatter and stratospheric LWIR emissions suggest changes in TEC, and measurement of ozone driven radiative change could provide a quantification of TEC variability. This is the crux of this research.

Over the last several years, the availability of new sources of data have broadened the current scientific understanding of the link between the ionosphere and stratosphere. This data has enabled researchers to focus on how disturbances in ion-drift variation alter the variability of lower-level electron density. By analyzing the trends of Global

Positioning System (GPS) TEC data during the occurrence of ionospheric disturbances, a tidal nature has been observed. These fluctuations associated with ionospheric disturbances are amplified during Sudden Stratospheric Warming (SSW) events. As early as 1993, stratospheric warming has been linked to global variations in zonal mean ozone, with evidence stemming from eight years of Solar Backscatter Ultraviolet (SBUV) data (Gonsharenko et al., 2010).

The link between stratospheric ozone and TEC variability is the semidiurnal migrating tide. The semidiurnal migrating tide develops as a product of solar radiation reacting with ozone and peaks at an altitude of around 45 km (Gonsharenko et al., 2012). The ozone distribution in this layer has been found to have a near Gaussian distribution in altitude. Observational data has indicated that the maximum ionospheric fluctuations actually occur several days after the peak in planetary wave activity, which could cause an offset in the timing of ozone's relationship with TEC variability. Ozone densities have been found to increase by around 25% and last for about 35 days after the SSW event (Gonsharenko et al., 2010). The spectral effects of this increase in ozone on radiation passing through the layer can be observed through LEEDR.

1.2. Background

The Earth's ionosphere is an upper atmospheric layer comprised partly of electrons and charged particles. While this region is heavily influenced by both geomagnetic and solar activity, roughly 20% of ionospheric variations can be linked with processes that take place in the lower atmosphere such as atmospheric waves and tides (Gonsharenko et al., 2012). Understanding this coupling is essential to ionospheric forecasting and broadening

the general knowledge of ionospheric plasma physics (Korenkov et al., 2012). Recent analysis of sudden stratospheric warming events has discovered a link to ionospheric fluctuations. Planetary tides are a primary driver of this coupling. Planetary tides cause a global circulation in which ozone is built up in certain regions. These regions experience an enhanced diurnal and semidiurnal tide. These waves increase in amplitude with height, and are able to influence the lower ionosphere and induce fluctuations in the TEC (Gonsharenko et al., 2012). The diurnal thermal tide is strongest near the equator while the secondary semidiurnal tide has a higher thermal amplitude in the mid-to high-latitudes (Forbes et al., 2008).

Ozone has several key spectral properties that are pertinent to its measurement. Ozone is greenhouse gas that plays a primary role in the absorption of solar UV radiation. It only constitutes 0.02 - 0.10 parts per million by volume within the atmosphere, but plays a key role in the energy balance of the planet (Bordi et al., 2015). About 90% of total atmospheric ozone is found in the lower stratosphere. The ozone absorption band centered at 9.6 μm is significant because it is spectrally near the peak in infrared emissions that are emitted by Earth. This infrared (IR) absorption region causes ozone to be a notable greenhouse gas. This absorption warms the lower stratosphere and cools the upper stratosphere above 10 hPa.

Ozone is also a strong absorber of solar UV radiation with wavelengths from 220 to 300 nm. The absorption spectrum of ozone peaks at 254 nm. The absorption of ozone in the UV spectrum leads to an increased level of radiative heating in the stratosphere. This creates a positive vertical temperature gradient, which leads to an increase in static stability. Solar UV radiation comes in three different subsets, which are based on their wavelength

and associated transmittance through the ozone layer. Ultraviolet A radiation is mostly independent of the ozone layer, with wavelengths in the range of 315 – 400 nm. Ultraviolet C radiation has wavelengths in the range of 100 – 280 nm and is completely absorbed by ozone in the atmosphere. Ultraviolet B radiation has wavelengths in the range of 280 – 315 nm and is absorbed by an amount that is dependent on the thickness and density of ozone that it is passing through. Because of this relation, the rate at which UV is absorbed can be used as a tool to measure ozone concentration. The spectral region from 300 to 330 nm is typically used to measure ozone concentrations in this fashion as ozone transmittance experiences the greatest differences in this band (Bordi et al. 2015).

Emissions from the Earth behave similarly to a blackbody at 288K. The emitted radiation from the Earth has a maximum at approximately 10 μm. Since ozone has a strong IR absorption band centered at 9.6 μm, it strongly absorbs this outgoing radiation and thus has a key role in the energy balance of the planet. This IR absorption band has a half width of .083 around this center (Kratz and Cess, 1988). Similarly to how ozone concentrations can be measured using UV radiation, satellites can use the amount of received IR radiation at the 9.6 μm absorption band to determine ozone concentrations.

1.3. Methodology

While there is a body of evidence showing that there is a relationship between upper stratospheric ozone and TEC variability, the majority of these studies have been event based and do not concern annual variations. Providing evidence of this relationship requires numerical data concerning both parameters for multiple sites and for long periods of time. There are a number of methods to acquire TEC estimates, however many do not have the

required resolution or support long-duration data requests. Upper stratospheric ozone can be acquired using specialized Brewer spectrometers.

After providing evidence to a link between stratospheric ozone and TEC, this study will use this relation to show how the spectral properties of ozone can be used to derive an estimate of TEC variability. This objective is accomplished using a program called LEEDR. LEEDR is a radiative transfer code which calculates spectral line-by-line and spectral band solutions. It utilizes terrestrial and marine atmospheric data as well as particulate climatology.

LEEDR is able to incorporate both observation-based and climatological atmospheric profiles, which can be adjusted to fit into a given scenario. This includes the alteration of individual gases to simulate possible changes in stratospheric ozone. If, for example, stratospheric ozone concentrations were to increase by a 25%, LEEDR can predict the spectral differences caused by this change. Using LEEDR, it is possible to estimate the effects that stratospheric ozone concentrations have on both UV and LWIR emissions. The findings are expected to show that changes in stratospheric ozone concentration will have observable spectral differences in both wavelength bands.

1.4. Problem Statement/Future Research

One primary goal of this study is to reaffirm empirical evidence for a relationship between TEC variability and thermal tide inducing 30 – 50 km ozone. Another is to examine whether a radiative transfer tool (LEEDR) would be able to quantify this change in ozone, and thereby characterize TEC variation. Evidence of a significant increase in upper stratospheric ozone can provide an estimate of TEC variability. Likewise, TEC

variability could be used to estimate ozone concentrations in the upper stratosphere. This finding would provide additional data sources of both TEC variability and stratospheric ozone concentrations in locations and time periods which would otherwise be inaccessible. Spectral emissions could also be used to confirm the onset of SSW events, which would be indicated by a very sudden and pronounced increase in stratospheric ozone. After further quantification of the effects of ozone variation, the goal will be to more accurately incorporate effects of lesser drivers into TEC models such as the Global Assimilation of Ionospheric Measurements (GAIM).

This document summarizes the current understanding of planetary tides and their effect on the ionosphere in Chapter 2. Chapter 3 outlines the motivation and methods in which data was acquired concerning diurnal TEC variation as well as upper stratospheric ozone. It also explains the process of incorporating ozone variations into LEEDR. Chapter 4 explores the impacts that ozone variability has on both LWIR and UV emissions. Chapter 5 investigates how this research can be incorporated into future work.

II. Literature Review

2.1 Overview

Before beginning a discussion regarding the influence of ozone on planetary tides and the resulting effect on electron densities, it is first imperative to consider why this influence is important. The TEC is an essential parameter of the ionosphere. The ionospheric composition is a critical consideration for over-the-horizon radars, electrical power grids, deep space tracking, satellite lifetimes, surveillance, and radio propagations (Schunk et al., 2012). The TEC fluctuations are also observed by the Global Navigation Satellite Systems (GNSS). Normally GPS signals are accurate to a range of a few meters, but these errors can reach higher than 100m during times of TEC variability due to strong geomagnetic storms. For these various reasons, TEC variations have been extensively researched and modeled with the investigation of the ionosphere and for physical applications. By considering the dispersive properties of the ionosphere, some error can be removed using dual-frequency systems like GPS. However, there are secondary effects that cannot be easily eliminated. One such effect is the dynamic coupling that the ionosphere experiences with the atmosphere below (Mukhtarov et al., 2013).

Due to the considerations involved with TEC variations, there is a growing need in civilian and military operations for both short-term ionospheric forecasts in the one to two day range, and long-term ionospheric forecasts in the four to five days range. Models are in development to meet this demand. The GAIM model has been developed by Utah State University and uses physics-based models of the ionosphere to produce short-term forecasts. Physics-based models have been created for the different levels of the ionosphere and atmosphere. These models are based the laws of physics that govern

motion in order to evolve density, flow velocities, and temperatures. They can include data driven, data assimilation, or coupled models. Data driven models use inputs derived from numerical measurements. Currently, short-term forecasts are best accomplished through data assimilation models. These are models that combine ionospheric measurements with the output of physics-based models to arrive at a combined state of the ionosphere. However, current physics-based and global ionosphere models are not advanced enough for long-term forecasts. Small errors in short-term forecasts amplify over time. One of the significant problems with long-term forecasts is the lack of understanding with lower atmospheric drivers. Physics-based models are not able to adequately describe large-scale ionosphere-thermosphere features (Schunk et al., 2012). If a solution to the inadequacies in ionospheric physics models is not found, it will be impossible to arrive at an accurate long-term ionospheric forecast. By more accurately assessing the smaller sources of variability, both short-term and long-term models will improve.

2.2 Tidal Theory

In considering the interaction of ozone's effects on the TEC, it is essential to understand how the ionosphere interacts with atmospheric waves from below. The types of waves that have the most impact on the ionosphere are planetary waves and thermal tides. Thermal tides are atmospheric oscillations on a global scale and consist of wind, temperature, density, and pressure. These tides have a significant impact on the dynamics in the lower thermosphere as they attain large amplitudes. Thermal tides are able to attain these large amplitudes because of the drop in atmospheric density with height combined

with energy conservation (Pancheva et al., 2012). Under normal conditions, tidal amplitudes become the largest atmospheric circulation in the region of the lower thermosphere.

The modern theory of atmospheric tides began to solidify nearly a half-century ago (Chapman and Lindzen, 1970). It was discovered that solar insolation absorption by ozone and water vapor are the two most important sources in the thermal excitation of tides. In addition, ozone was shown to be considerably more important in generating semidiurnal oscillations. The reasoning for this is that the ozone excitation occurs at a higher altitude and through a greater depth. Water vapor is more strongly connected to diurnal heating and associated diurnal oscillations, which causes greater impacts near the equator where the most direct solar radiation is observed. Early indications were that the transmission of the daily variations of ground temperature to higher altitudes through the means of turbulence and radiation are comparatively small. This theory was backed by the observational evidence available at that time. The thermal variations of the land and sea would produce thermal tides that do not follow the sun. This non-migrating component of tides was originally observed to be insignificant compared to the migrating counterpart (Chapman and Lindzen, 1970). Newer studies conducted in the 2000s would argue that this is not always the case. In some instances, non-migrating tides have been found to exceed their migrating counterparts (Pancheva et al., 2012).

Studies into the dynamics in the lower to mid-levels of the atmosphere have been limited due to both the limited range of sounding instruments and the associated interests of researchers. Thanks to the introduction of more sophisticated instrumentation and further evidence of an atmosphere and ionosphere link, that is beginning to change.

Some of the initial research used data accrued from the Nimbus 6 satellite to investigate the coupling between the stratosphere and higher levels of the atmosphere (Lawrence and Randle, 1996). This study showed wave-like events that were observable through multiple levels. Studies like this one have furthered the understanding atmospheric and ionospheric coupling. This improvement is due primarily to observations from ground-based radars and optical sensors as well as new instrumentation onboard satellites (Pancheva et al., 2013). These measurements have led to the conclusion that the environment is dominated by large-amplitude atmospheric waves.

Another instrument used to gain insight on the connection between the ionosphere and the atmosphere is the Climate and Weather of the Sun-Earth System (CAWSES II) program. CAWSES II is an international program initiated by the Scientific Committee on Solar-Terestrial Physics (SCOTEP). The goal of this program was to answer some of the major questions that remain regarding atmosphere and ionosphere interactions (Oberheide et al., 2015). One of four task groups associated with the program was specifically given the charge of shedding light on the dynamic coupling between the low and middle atmosphere. Specifically, this task group sought to examine tidal structures between 110 and 400 km, tidal impacts on the energy balance in the thermosphere, and tidal coupling of the E and F region. It has now been theorized that in addition to modulating the E-region dynamo, the coupling between tides and the ionosphere can be attributed to thermospheric [O] to [N] ratios, neutral density variations, and meridional winds in the F-region (Oberheide et al., 2015).

The most significant source of tides in the lower thermosphere is atmospheric heating as a result of the absorption of solar radiation. This absorption is primarily

induced by stratospheric ozone and tropospheric water vapor, although the latter is mainly significant at low latitudes (Jones et al., 2014). Water vapor is confined mainly to the lower troposphere, and heating generated by this molecule decreases exponentially with height to the point that its impact is insignificant in the middle atmosphere (Lal, 2001). Part of these atmospheric variations due to heating manifest themselves in the form of migrating tides, which propagate with the motion of the sun and are dependent only on the time of day. Other tidal variations do not depend of the motion of the sun and are dependent on other factors such as longitude; they result in a non-migrating tide. Non-migrating tides arise from at least two different mechanisms. One is zonally asymmetric forcing that can arise due to geographic dependent heat sources, topography, or differences in longitudinal solar heating. The other mechanism is the nonlinear interaction between migrating tides and stationary planetary waves (Jones et al., 2014).

Vertically propagating solar thermal tides finally begin to dampen in the lower thermosphere as they become subject to eddy and molecular dissipation. Dampening occurs at altitudes between 100 and 120 km and tidal amplitudes are at a maximum just before this level. This corresponds to the E-region in the lower ionosphere. As migrating and non-migrating tides dissipate, they deposit their momentum and energy into the region, and modify the mean circulation. This effect can modulate the large-scale circulation pattern. This thermal dissipation is how the lower atmosphere is connected to the middle and upper atmosphere. This oscillation also interacts with other less significant waves at this level such as gravity and planetary waves to further generate wave activity. As tides enter into the E-region, they can affect the higher F-region through the E-region wind dynamo (Pancheva et al., 2012).

Through the E-region wind dynamo, lower thermosphere dynamics are able to influence the ionospheric F-region. These dynamics are described by a sequence of processes. First, the tidal winds transport positive ions by way of collisions while electrons stay fixed to their magnetic field lines. This separation of charges creates an electric current. In accordance with Maxwell's steady state equations, a polarization electric field is established to maintain non-divergent flow (Forbes et al., 2008). Polarization electric fields then travel from the E-region to the F-region through equipotential magnetic field lines, and have been found to propagate completely vertically (Pancheva et al., 2012). Tidal wind shear in the E-region is instrumental in creating ionospheric intermediate layers, which is called sporadic E. Sporadic E has been found to be dependent on diurnal and semidiurnal tides. This process allows lower thermospheric tides to effect the whole ionosphere system.

Planetary tides refer to the solar tides that occur within the atmosphere and ionosphere. They can be migrating, which means that they move in response to the Sun's motion. Planetary tides can also be non-migrating, which do not follow the Sun's motion. Tides that are able to affect the ionosphere propagate from below and constitute the vertical coupling in the atmosphere (Laštovička, 2006).

2.3 Thermal Tide Generation

Planetary tides have a noteworthy impact on the large scale dynamics of the atmosphere. Like all waves, tidal components grow in amplitude as altitude increases because the atmospheric density decreases and energy is conserved (Pancheva, 2013). Tidal forcing is mainly a product of thermally driven processes. The heating that excites

the tides is caused primarily by the absorption of solar radiation by ozone in the stratosphere, with other sources being water vapor in the troposphere and [O_2] in the lower thermosphere. Heating occurs during daylight hours, and is dependent on height as well as atmospheric composition. This uneven heating caused by the change from day to night is what gives rise to migrating atmospheric tides. At some point as these tides propagate vertically, they will be forced to dissipate. The tides deposit their energy at these higher altitudes resulting in atmospheric and ionospheric variations.

These thermally driven atmospheric tides exhibit primary periods of 24 hours (diurnal) and 12 hours (semidiurnal), and have been observed for decades. In addition, there are even 8 hour (terdiurnal) and 6 hour (quad diurnal) tides that have been observed with smaller amplitudes (Gong et al., 2013). Semidiurnal tides can be observed as two maxima and two minima occurring every day at near the same solar time, which indicates that they have a solar origin. Semidiurnal tides have also be observed to be the main tidal response at most latitudes. However, the main solar forcing is physically diurnal in nature, which brings the previous statement into question. This contradiction was answered through two primary observations. The diurnal signal is unable to propagate down to the surface at latitudes poleward of 30°N and 30°S since due to the shorter pendulum day. In addition, vertically propagating waves have a comparatively shorter vertical wavelength and are prone to destructive interference (Whiteman and Brian, 1996). This indicates that semidiurnal tides within the atmosphere are primarily thermal based. In addition, there are also those that are gravitationally based which may also effect the ionosphere. Tidal effects on the ionosphere arise due to perturbations in both neutral composition and dynamics (Laštovička, 2006).

Planetary tides are strongly attributed to ozone's absorption of solar radiation. Near the equator, where diurnal migrating tides are at their peak, maximum ozone heating typically occurs at altitudes near 45 km and important contributions of ozone heating can be seen at altitudes down to 30 km (Pancheva, 2013). However, electron densities in the ionosphere do not become substantial until closer to 100 km in altitude. This difference in altitude could intuitively lead one to dismiss ozone's potential impact on the ionosphere. However, ozone heating in the upper stratosphere induces a thermal tide that is able to propagate into the thermosphere. Planetary tides can propagate upwards in altitude until they are dissipated by ion drag, molecular diffusion, and eddies. This occurs in the lower ionosphere-thermosphere at altitudes between 80 and 160 km, where they transfer energy and momentum into the system (Jones, 2014). In fact, upward-propagating tides have been shown to reach their maximum amplitudes in the lower thermosphere at around 90 – 120 km where they are then dissipated in the E wind dynamo region.

Evidence shows that ozone and its associated migrating tides are enhanced during SSW events. SSW events can be observed in the winter within the stratosphere, and are caused by interactions between planetary waves and zonal winds. Planetary waves transport ozone poleward from near the equator. This transport results in spikes in zonal ozone concentrations at low latitudes. Ozone variabilities in the stratosphere were recorded during major SSW events in 2006 and 2009. In both high and low latitude cases, ozone concentrations above 85 km were shown to decrease during the event and gradually recover by the end of the event. At lower altitudes near 36 km, and closer to where the peak stratospheric ozone heating occurs, the opposite effect was observed

(Sridharan, 2012). This relationship during warming events has been observed for decades (Randel, 1993).

2.4 Migrating and Non-migrating tides

Atmospheric solar tides are at a global-scale, and have periods which are harmonics of a solar day. These tides can be excited through a number of ways. Possible sources of excitation are the absorption of solar radiation, latent heat release, interactions of global-scale waves, gravitational pull from the sun, and the interaction of tides with gravity waves as they become unstable in the lower thermosphere (Hagan and Forbes, 2003). Semidiurnal solar tides are a subset of solar tides with a period of 12 hours with a perturbation maxima and minima along a longitudinal axis. Solar tides can either be migrating or non-migrating. Migrating tides propagate with the motion of the sun as observed on the ground. Non-migrating tides can be described as perturbations that do not follow the motion of the sun. Migrating tides maximize at the same local time for all longitude at a particular latitude. Non-migrating tides on the other hand can be seen as longitudinally based fluctuations of wave amplitude and phase (Friedman et al., 2009).

The semidiurnal migrating tide is primarily the result of the absorption of solar radiation by stratospheric ozone. Disturbances to the overall stratospheric circulation can have a significant effect on the distribution of stratospheric ozone, and thereby the semidiurnal tide. An analysis of a December 2008 event at 2 hPa (~43.5 km) showed that low latitude ozone densities dramatically increased (Goncharenko et al., 2012). This increase in stratospheric ozone densities was true for the upper stratosphere above 30 km with a peak increase of 25% from 40 – 45 km. This is why SSW events can be connected

to atmospheric tides and ionospheric variations. On the other hand, lower stratospheric ozone densities below 30 km decreased on the order of 5%. This variation in mean ozone is in agreement with earlier studies including one based on eight years of SBUV data (Randal, 1993). This variation between lower and upper stratospheric ozone can be understood through meridional circulation cells induced by planetary waves (Randel, 1993). Forcing in the high-latitude winter hemisphere forces a circulation with a clockwise lower cell below 40 km, which is oriented towards the north near this altitude, and a counter clockwise upper cell above 40 km.

While non-migrating and migrating tides have been studied for decades, satellite evidence has only recently measured their impacts. The Sounding of the Atmosphere using Broadband Emission Radiometry (SABER) was used over a 4-year study from March 2002 through December 2006 to quantify the tidal amplitudes due to migrating and non-migrating waves. This sensor is onboard the Thermosphere Ionosphere Mesosphere Energetics Dynamics (TIMED) satellite. The satellite experiences a 96 minute period orbit, and pairing this with the rotation of the Earth results in 15 orbits being sampled per day. SABER data was processed with 60-day windows and a Fourier fit with respect to longitude to arrive at temperature and stationary wave components. Because of this 60-day window, coherent and consistent waves must exist over this time for the data to be represented. Measurements based on this long-term average will limit the incoherent effects of gravity and planetary waves (Friedman et al., 2009). Day-to-day variability of thermal tides may be underestimated in this region due to the moving average.

Measurements from SABER show that tidal amplitudes vary with latitude (Figure 1). The diurnal tide exhibits small amplitudes near 20° with maximas located at the equator and near 30°. The semidiurnal tide is typically very strong in the subtropics, with fluctuates between 8 and 16K (Forbes et al., 2008). Observed SABER radiances used to acquire temperature data consisted of lower level temperatures, the rate of [CO_2] deactivation by [O], and several other rates. Relying on [CO_2] and [O] densities to calculate lower level temperatures induces error into the upper level temperature calculation (Forbes et al., 2008). SABER makes temperature measurements at altitudes coincide with the capabilities of LIght Detection And Ranging (LIDAR) remote sensing. This allows for the opportunity to compare data between the two (Friedman et al., 2009). A study at stations in Puerto Rico and Hawaii revealed that LIDAR observed temperature amplitudes are slightly larger in general than those observed by SABER, though there was some seasonal variability. This difference can be explained by the long measurement window used by SABER (Friedman et al., 2009).

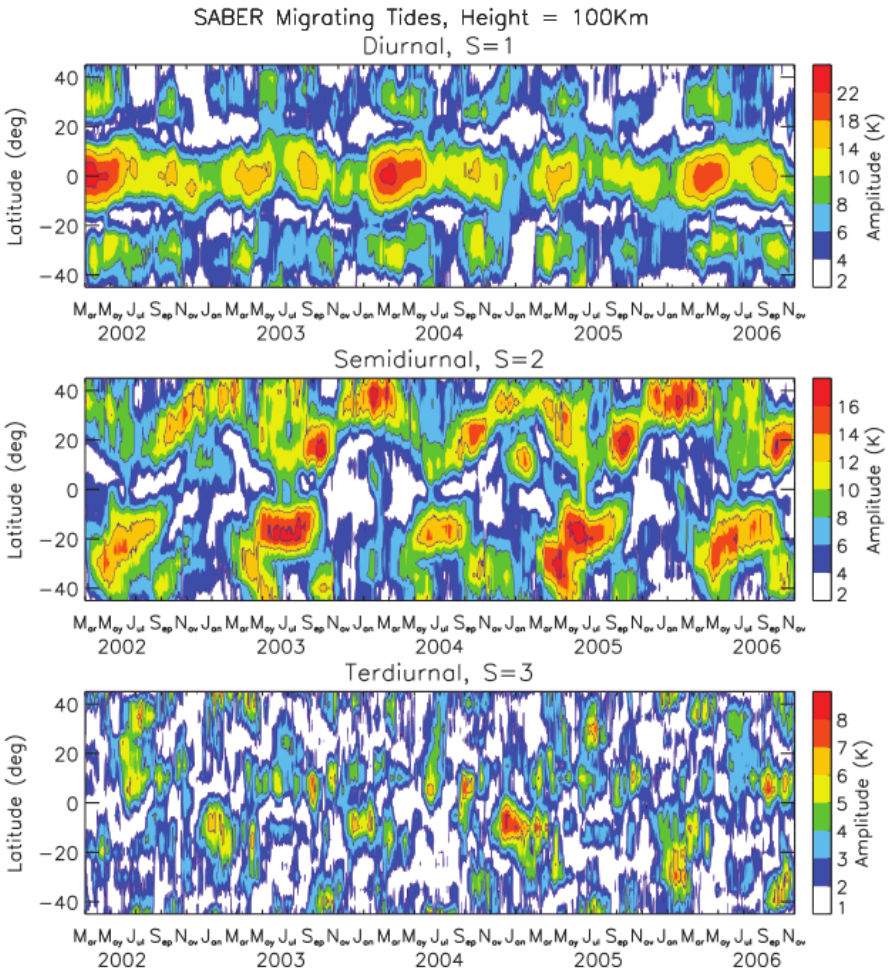

Figure 1: Migrating Tides Thermal Amplitudes (Forbes, 2008)
Diurnal, semidiurnal, and teridiurnal thermal amplitudes at 100 Km for latitudes between 45S and 45N. Based on SABER measurements conducted from Mar 2002 through November 2006.

While space weather in Earth's near space environment has traditionally been thought to be caused entirely by solar energy injections at high-latitudes, the geospace has been found to be strongly linked to terrestrial weather below (Oberheide et al., 2013). As tidal theory progressed, it was discovered that non-migrating tides are extremely important in generating longitudinal irregularities in the ionosphere system (Oberheide et

al., 2013). Satellites would later confirm this hypothesis and helped to supply a foundation of quantitative knowledge regarding tidal forcing and propagation.

Non-migrating tides have been theorized to arise from a number of different factors. One of these factors is landmass, which has been observed to modulate the forcing of thermal tides. This effect is due to land generating more atmospheric heating than oceans. This nonuniform forcing results in non-migrating tides and stationary planetary waves are theorized to result in waves that do not follow the motion of the sun (Friedman et al., 2009). Another two theories concerning the sources of non-migrating tides are non-linear interactions between planetary waves and migrating tides and the presence of longitudinally varying ozone and water vapor (Forbes et al., 2003). Another significant source of non-migrating tides is theorized to be latent heat release resulting from deep convective systems. Latent heat release associated with these systems is greatest in the equatorial tropics (Oberheide et al., 2002). Currently it is difficult to assess the degree to which each of these factors influence non-migrating tides.

Migrating tides with periods of 12 and 24 hours have been the primary targets of planetary tide research, but terdiurnal (8 hr) tides have been observed as a direct result of solar radiation incident upon different latitudes. This component is the third harmonic of the Fourier decomposition of time, and has usually been ignored because its amplitude is typically smaller than diurnal tides. However, there are occasions in which the terdiurnal tide is amplified and becomes more analogous. This component has regularly been seen by ground-based instruments located near the mid-latitudes (Pancheva, 2013).

Migrating and non-migrating tides have been incorporated to an extent in ionospheric models, such as GAIM, as a large scale forcing mechanism. However,

evidence suggests that migrating tides significantly attribute to the formation of smaller scale features that models may have a harder time resolving. Of particular importance in the low to mid-latitudes is thermal tide's role in the formation of plasma bubbles. Both diurnal and semidiurnal tides are theorized to force the dominant neutral motion field within the F-region. Modulations in these motions have been evidenced to accompany the onset of plasma bubbles (Fritts et al., 2009). Tidal structures exhibit large amplitudes in the lower thermosphere, and are expected to transfer this instability to plasma bubbles.

2.5 Past Research and Data

A number of ionospheric models have been introduced to capture the impact of planetary tides. A study conducted by Fensen (1997) simulated the tidal-induced perturbation on the F-region ionosphere using the thermosphere-ionosphere-electrodynamic general circulation model (TIEGCM). The investigation was conducted using the TIEGCM simulated average solar minimum conditions and quiet geomagnetic conditions for the month of March. The model was run using three separate forcing mechanisms. The first considered only solar forcing, the second added auroral activity effects, and the third considered solar forcing combined with tidal effects. The introduction of tidal effects differed greatly from the pure solar forcing result. Not only were electron number densities affected by up to 40% at certain latitudes, but the altitude of maximum electron density also varied by up to 30 km (Fesen, 1997).

A study by Goncharenko explored the most notable characteristics for ionospheric variability during SSW events (Goncharenko et al., 2010). SSW events are of particular interest because they are easily identified by thermal profiles and are accompanied by

strong fluctuations of the TEC. Both migrating and non-migrating tides are enhanced during SSW events. They are considered primary examples of strong coupling that exists between different atmospheric levels (Goncharenko et al., 2012). The study consisted of a single event in January 2009, and focused on 75W longitude and latitudes between 40S and 40N. As an equatorial ionization anomaly became well-developed during the SSW event, TEC values spiked by roughly 10 – 15 TECU (10^{16} electrons/m^2) in comparison with the 10-day mean. Six hours later, TEC values had decreased to approximately 10 TECU below the 10-day mean. A secondary increase in TECU was observable six hours later. The semidiurnal perturbation amplified and reached a maximum several days after the SSW peak occurred and lasted for several weeks (Goncharenko et al., 2010). This study provided yet further evidence of a strong link between the lower and upper atmosphere.

In another analysis of the Dec 1, 2008 – Mar 1, 2009 SSW event, the focus was on SSW's relation to ozone and the resulting impact to temporal and special evolution of planetary wave activity. This study focuses on the impact to the distribution of stratospheric ozone, which in turn generates the semidiurnal migrating tide. The peak in ozone density strongly correlates with the strength of the SSW event and increases by as much as 25% between 40 and 45 km (Goncharenko et al., 2012). The study attributed this increase in stratospheric ozone to three different mechanisms. They are the upward transport of ozone from lower altitudes, meridional transport between hemispheres, and a longer ozone lifetime resultant from tropical upper stratospheric cooling.

Shining a light on the current capability of ionospheric models, the values of the International Reference Ionosphere (IRI) model were compared to the TEC data collected

by GPS. In this instance, IRI TEC values overestimated the GPC TEC by roughly 30%. This difference can be mainly attributed to the extremity of the solar minimum at the time, but the model sufficiently captured the diurnal variation in TEC values. The main difference between the model and the data is the extreme variability observed during the daylight hours in the data. This sudden change in the variance of the GPS TEC values is not reflected by the planetary K index which characterizes the magnitude of geomagnetic storms. This indicates that geomagnetic storms were not responsible for this variance. This strongly suggests that the ionosphere responds to modified tidal forcing (Goncharenko et al., 2012).

Other studies have investigated the amplitudes and periods of planetary waves and tides at high altitudes. Planetary tides have large spatial extents and long periods, which coincide with variations in the F-layer. In fact, these waves can have periods extending from two to 16 days and have a longitudinal scale that spans thousands of kilometers (Rishbeth, 2006). Such results give rise to the expectation that increases in thermal amplitudes can have long lasting and widespread effects. This period is in line with the increased TEC observed by Goncharenko during SSW events (Goncharenko et al., 2010).

2.6 Properties of Ozone

To gain greater insight regarding variations in stratospheric ozone, it is helpful to understand how and why ozone forms. In 1930, Sidney Chapman devised an explanation for stratospheric ozone that consisted of a four-reaction process. Ozone is produced through the photolysis of oxygen molecules into oxygen atoms in the first reaction

equation. The individual oxygen atoms interact with another oxygen molecule to form ozone in the second reaction equation. This process requires that excess energy be removed by a third body and is denoted here in the reaction equation term as M, and is just another molecule in the atmosphere. When added together, the net reaction shows that oxygen atoms and ozone are created when oxygen molecules are exposed to UV light (Middlebrook and Tolbert, 2000). This photochemical production mechanism is the only source for creating ozone.

On the other hand, ozone can also be destroyed when it is exposed to light, breaking down into oxygen atoms and molecules as shown in the third reaction. This process does not necessarily lead to the destruction of ozone because these particles can recombine into ozone through the second reaction. Ozone can also interact with an oxygen atom to create two oxygen molecules. This decomposition process forms a net reaction where two ozone molecules decompose into three oxygen molecules when exposed to light.

$$O_2 + \text{UV Light} \rightarrow O + O \qquad \lambda < 242\text{nm} \tag{1}$$

$$O + O_2 + M \rightarrow O_3 + M \tag{2}$$

$$\text{Net: } 2\,O_2 + \text{UV Light} \rightarrow O + O_3$$

$$O_3 + \text{ Light} \rightarrow O_2 + O \qquad 240 < \lambda < 310\text{nm} \tag{3}$$

$$O + O_3 \rightarrow 2\,O_2 \tag{4}$$

$$\text{Net: } 2\,O_3 + \text{Light} \rightarrow 3O_2$$

Taken as a whole, these four reaction equations describe the production and loss of ozone, and is called the Chapman mechanism. The total amount of ozone observed in the real world is less than what is predicted by the Chapman mechanism. This is because there are other methods in which ozone can be destroyed besides the fourth reaction. In fact, there are several kinetic reactions that are able to destroy ozone. For example, in the 1970s it was discovered that ozone is destroyed in a cycle that involves nitrogen oxides described by reaction equations five and six. The net change from this reaction is ozone and oxygen atoms breaking down into two oxygen molecules (Middlebrook and Tolbert, 2000). Hydrogen oxides were found to have a similar effect. Observable stratospheric ozone concentrations are the result of the balance between these production and deconstructive chemical processes. This balance is determined by a number of factors such as altitude, sunlight intensity, and temperatures. When conditions favor ozone production and limit its decomposition, ozone increases in abundance and is a reason why the ozone layer fluctuates in altitude.

$$NO + O_3 \rightarrow NO_2 + O_2 \quad (5)$$

$$O_2 + NO_2 \rightarrow 2\,NO + O_2 \quad (6)$$

Net: $O + O_3 \rightarrow 2\,O_2$

Temperature variations can significantly affect ozone variability. This is because there is an associated temperature dependence of ozone chemical reactions. Cooling leads to an increase in ozone, and this is because the reactions that cause the destruction of ozone are slowed down. Tidal winds can vertically transport substantial amounts of

atomic oxygen. In fact, in extreme cases this vertical transport can amplify the atomic oxygen concentration by an order of magnitude. Because the chemical production of ozone is related to atomic oxygen, this tidal transport can also affect ozone variability (Pancheva et al., 2014).

The peak heating altitude of ozone has been observed at an altitude of around 45 km; however, the peak density of ozone is located closer to 21 km. The reason for this difference is that ozone absorbs solar energy mainly at altitudes above its density maximum. Ozone is a strong absorber in several wavelength bands termed the Hartely, Huggins, and Chappuis bands. Heating rates due to absorption in the Huggins band is highest between 30 and 50 km, while heating rates in the Hartley band sharply peaks at around 45 km. Heating rates due the Chappuis band are less significant and peak at about 35 km. Taking into account the combined contribution of these absorption bands, heating rates due to ozone occur primarily above 25 km and maximize around 45 km (Lal., 2001). It is also worth noting that ozone in the stratospheric region also produces a cooling effect. However, cooling associated with ozone is much less than other molecules found in this region.

The point of the discussion up to this point has been to establish a link between solar tides and stratospheric ozone to electron density variability. However, it is also possible to observe the overall effect that planetary tides may have on the magnitude of electron densities. At lower latitudes, a 13% decrease in [O] and 16% increase in mean [O_2] was measured as a result of upward propagating tides. This change was found to extend upwards into the F-region of the ionosphere where the decrease in [O] was still at 10% and the increase in [O_2] of near 30%. In the F-region, oxygen ions play a dominant

role in the change of electron densities concentrations. The result of a decrease in atomic oxygen concentration leads to a net decreases in the electron density production and thereby a loss in electron density concentrations. A decrease in mean electron density of up to 25% was found within the F-region due to this reduction in atomic oxygen (Jones et al., 2014).

2.7 Ozone Measurement Techniques

The use of ozone as a secondary tool to be used in determining electron density variability is contingent on the fact that ozone concentrations are readily available. There are two types of ozone measurement: in-situ and remote. In-situ ozone measurements consist of an instrument being locally exposed to the atmosphere at the altitude at which it is measuring. Once the ozone is inside the instrument, it is measured by its absorption of UV light or the current resultant of the ozone chemical reaction. Through 1986, balloon-launched ozonesondes locally measured ozone at nine stations, but the balloons were limited to an altitude of around 30 km where they are halted by the stratopause. In addition, high-altitude research aircraft are able to reach the ozone layer at many locations throughout the globe.

The first means of remotely measuring atmospheric ozone was the Dobson spectrometer. These spectrometers were introduced in the 1920s and are currently still in use. There have been more than 30 worldwide stations measuring the total ozone thickness since 1957 (Stolarski et al., 1992). The bulk of these stations are located in the Northern Hemisphere. This instrument is ground based and measures solar radiation transmitted at pairs of wavelengths in the UV near 300 nm. One of these wavelengths is

placed in a significant absorption line, while the other is attenuated by an optical segment. The optical segment is then moved so that the two beams achieve an equal signal. Measurements are taken for distinct pairs of wavelengths so that the error associated with additional aerosols can be eliminated. Data collected from these various stations are reported to the World Ozone Data Center located in Toronto, and are published every month (Stolarski et al., 1992).

Beginning in November 1978, total ozone has been measured on a near global basis using the Total Ozone Mapping Spectrometer (TOMS), which was first installed on the Nimbus 7 satellite. TOMS works by measuring the Earth UV albedo at wavelengths around 300nm. Early measurements were affected by a problem with the diffuser plate that was used to determine Earth's albedo. Early ozone data collected from TOMS has been corrected for the darkening that was gradually exhibited by this diffuser plate. The data set after being adjusted is estimated to being precise within ± 1.3% (Stolarski et al., 1992).

Analysis of ozone and meteorological information gathered in the 1990s suggest that there is also a solar cycle variation of stratospheric ozone and temperatures. A thorough investigation of the Solar Spectral Irradiance (SSI) has shown that during periods of low solar activity, there is an associated increase in SSI for wavelengths longer than 502 nm and decrease in SSI for wavelengths shorter than 502 nm (Bordi et al. 2015). During the declining phase of the solar cycle, stratospheric ozone values at altitudes less than 45 km are reduced in general. However, stratospheric ozone data observed over the last three solar cycles from 1979-2013 show that the upper stratospheric ozone concentrations were out of phase with the solar cycle (Bordi et al., 2015).

The Backscatter UV (BUV) instrument debuted on April 1970 onboard NASA's Nimbus 4 satellite. Since then, nine additional instruments of gradually improved design have been launched between NASA and NOAA. Satellites oriented towards the Earth are also able to observe UV radiation backscattered by the atmosphere. This is a technique is called SBUV, which was previously mentioned. Ozone sensing instruments included onboard the Nimbus 7 used twelve wavelengths within the 250 to 340 nm band. Using these different wavelengths, one can calculate the vertical distribution and density of ozone. The SBUV consists of an instrument series installed on three NASA and seven NOAA satellites of which three are currently in operation (Bhartia et al., 2013).

2.8 TEC Measurement Techniques

The TEC is defined as the integral of electrons along a raypath and its unit is the TECU, which is 10^{16} electrons/m^2. It can be computed using either bottom or top side ionosondes. Estimates of TEC can be derived from faraday rotation of satellite signals such as the Russian Global Navigation Satellite System (GLONASS), European Incoherent Scientific Association (EISCAT), from double frequency altimeters, and from GPS phase/delay recordings (Nayir et al., 2007). These measurement systems all have different integration paths, and direct comparisons are problematic. Since the 1990's, dual frequency GPS has been used for regional and global TEC estimates.

GPS satellites are the system of choice due to their large number and global coverage, and their 20,000 km orbit ensures they can capture the entire ionosphere. GPS signals are also high enough to minimize the effect of the magnetic field surrounding the Earth and ionospheric absorption. Receivers at GPS stations transmit at two frequencies,

one at 1575.42 MHz and the other at 1227.60 MHz (Nayir et al., 2007). The time for the signal to propagate through the ionosphere is recorded as a pseudo range. TEC is calculated by fitting the difference in the two pseudo ranges to the difference in the carrier phase delay. This calculation is relatively simple; however, the TEC calculation is often obscured by noise and multipath signals, which add error to the result (Nayir et al., 2007).

There are a number of methods used to fit the pseudo ranges to carrier phase delays to derive a TEC estimate. The main differences between them is how they solve for different sources of error. All available methods suffer from cycle slip issues when the GPS receiver loses satellite lock. The estimate of TEC must also account for interfrequency bias due to the instruments themselves. Because TEC bias is calculated differently in each of these methods, TEC estimates vary by model (Nayir et al., 2007).

Regularized Estimation of TEC (Reg-Est) is one model for high-resolution thorough TEC estimation. Data is obtained in IONosphere Map Exchange Format (IONEX) from International GPS Service for Geodynamics (IGS) centers. Initially, the Slant Total Electron Content (STEC) values are computed for all available satellites above 10 degrees from the horizon at intervals of 30 seconds. Reg-Est assimilates the processed signals in a least-squares sense to estimate the Vertical Total Electron Content (VTEC) over a chosen duration. Multi-path contamination is reduced by assigning a weighting function on the computed TEC using satellite position and local zenith. The error associated with multi-path scattering is particularly significant at low elevation angles. A regularization algorithm then combines both the computed and weighted VTEC into a single smoothed VTEC. Reg-Est produces TEC estimates for all latitudes and

ionospheric conditions. The IGS center utilizes a 2-hour global TEC map, while the Reg-Est computes TEC at one station at 30-second intervals (Nayir et al., 2007).

2.9 Radiative Transfer (LEEDR)

Assuming that there is a substantial link between stratospheric ozone and TEC variability, measuring either stratospheric ozone or TEC variability should allow one to arrive at a baseline estimate of the other. Because ozone is a strong absorber in the UV and IR spectrums, it is possible to achieve an estimate by simply observing the path radiance through the atmosphere. Observing path radiances can be accomplished using radiating transfer algorithms.

Radiative transfer algorithms calculate the electromagnetic radiation that propagates through a planetary atmosphere. These codes vary in the extent of their scope, incorporated models, and derived output. LEEDR is a particularly robust program that can incorporate real-world data and can be adjusted to fit many geographic locations and scenarios. LEEDR derives molecular absorption by combining line strength data from the High Resolution Transmission (HITRAN) 2008 molecular absorption database with constructed vertical profiles. For wavelengths shorter than 1 mm, LEEDR assumes a Lorentzian distribution for pressure broadening of absorption lines. Alternatively, for wavelengths of greater than or equal to 1 mm, the Van Vleck-Weisskopf distribution is used for the line shape. LEEDR supports wavelengths from 200 nm to 8.6 meters. The user is also able to select 16 different cloud and precipitation types (Fiorino et al., 2013).

LEEDR allows graphical access and export of the Extreme and Percentile Environmental Reverence Tables (ExPERT) database. This allows LEEDR to generate

more realistic profiles that take into account factors such as moisture and humidity on aerosol distributions. Over the world, there are 573 surface sites to choose from. LEEDR also has the capability of ingesting surface data to create a more realistic data profile (Fiorino et al., 2013). In addition to generating a vertical profile, LEEDR is capable of querying past records through the NOAA National Operational Model Archive and Distribution System (NOMADS). NOMADS queries GFS numerical weather data and combine it with a climatological basis for aerosols and turbulence, which allows LEEDR to produce a more realistic and near real-time atmosphere.

2.10 Summary

This section has highlighted the significant findings regarding the development and current application of tidal theory, the chemical and radiative properties of ozone, ozone measurement techniques, TEC measurement techniques, and radiative transfer models. This section also covered past research studies that linked atmospheric tides to ionospheric disturbances. An investigation into past research shows that while short-term events such as SSW have been investigated at low latitudes for its ionospheric effects, there are few studies that cover a substantial length of time. Considering these findings, research is needed to determine if stratospheric ozone can be correlated to TEC variability at different latitudes and for a longer period of time. It also needs be considered whether these changes in stratospheric ozone density can be observed in the effect it has on the radiative paths in the UV and IR absorption bands.

This background information shows how it is possible for atmospheric tides to have substantial impacts to the ionosphere and how ozone is able to impart change on

tides. It also shows that radiative transfer programs can be used to construct molecular absorption profiles for the atmosphere, and that by altering one of these absorbers, there should be an impact to the resulting radiative spectrum. Therefore, it should be possible to observe the effect that a change in stratospheric ozone has on spectral backscatter and emissions. In addition, now that the stratospheric ozone and TEC variability connection has been shown to be plausible, it is necessary to actually collect and compare this data. This is what the next chapter will cover in detail.

III. Methodology

3.1 Overview

This chapter explains the reasoning and methods used to collect and analyze the data presented in this study. The first objective was to capture data that either supports or denies stratospheric ozone's contribution as a significant contributor to TEC variation. This requires stratospheric ozone data, raw satellite data, and a program to convert the raw satellite data into a TEC profile. Topics in this section include descriptions of the various data collection sources, the way in which the data is gathered, and the rationale behind the selection of those particular sources. This section will also discuss the various purposes of this data as well as any inherent limitations.

3.2 Using LEEDR

If a clear relationship between TEC variability and ozone exists, it opens the possibility for TEC variability to be estimated from examining spectral emissions. LEEDR is a radiative transfer code used for calculating line-by-line and spectral-band solutions. It accomplishes this by creating realistic profiles of meteorological and environmental effects. Changing the atmospheric constituents changes the absorptive and emissive properties of the atmosphere. Ozone has particularly strong absorption bands in the UV and IR, which will be vital in capturing backscatter's relation with ozone fluctuations. As a radiative transfer tool, LEEDR can be used to characterize this effect by investigating how it is affected by an incremental change in stratospheric ozone.

When recreating the atmospheric profiles for use in computing radiative transfer, LEEDR allows for the selection of data from various sources. One of these sources is

NOMADS, which is a data repository that is used to collect GFS weather data in addition to climatological normal aerosols and turbulence to mirror a more realistic atmosphere. The GFS data collected by LEEDR is mapped on a 3-D grid with .5-degree resolution with 3-hour time intervals. Another data source LEEDR can pull from is ExPERT, which is another useful model that provides an improvement upon a standard atmospheric profile. ExPERT is based on correlated, probabilistic surface climatology that is particular to a requested location. Additional ExPERT features include being able to select by season, time of day, and relative humidity. For these reasons, ExPERT was the pick for the model in this study.

LEEDR incorporates various atmospheric aerosols through four Moderate Resolution Transmittance (MODTRAN) models in addition to the Global Aerosol Data Set (GADS). MODTRAN is a radiative transfer algorithm that is used to model the absorption, transmission, and emissive properties of the atmosphere. The propagation of electromagnetic radiation is affected by the scattering and absorption by both air molecules and aerosols. Aerosols can vary significantly in their concentration, size, and composition and all of these factors effect IR radiation. In addition, there is a need to estimate the transmittance, sky radiance, and other atmospheric optical effects (Shettle and Fenn, 1979). This is why models for atmospheric aerosols are necessary in accurately estimating radiative transfer. Using MODTRAN, aerosols are modeled using 10 components describing their relative size, distribution, and spectral indices. Optical properties are calculated using Mie-Theory for wavelengths between .25 and 40 μm. Mie theory is the collection of the Mie solutions and methods to Maxwell's Equations, which

describe how electromagnetic waves are scattered by homogeneous spheres Shettle and Fenn, 1979).

The following is a summary of how the LEEDR atmospheric profile was adjusted. Upon selecting to use either NOMADS or ExPERT as the data source of choice to create a profile, the user must then select the number of layers along with the height of the atmosphere. In order to construct the total profile, the molecular effects of the various atmospheric gases are summed together after calculating each gas individually. It is also possible to isolate ozone from the calculated profile, adjust these values according to the TEC and ozone relationship, and then feed these altered values back into the equation.

When a profile is created in LEEDR based on one of the aforementioned models, ozone as well as other atmospheric constituents is input in their relative numerical concentrations throughout the profile. By modifying the ozone densities at the desired levels, absorption and emission for the atmospheric spectrum will also change. For ozone, this will be most apparent for absorption in the UV spectrum between 200 and 350 nm and absorption in the IR around 9.6 μm. In these wavelength bands, ozone is a particularly strong absorber. Provided that TEC variability and ozone relationship follows the findings previously discussed research, it follows that changes in this absorption band can be linked to electron density variability.

One of the keys to this research is that stratospheric ozone can be adjusted in order to see the resulting radiative effects. In order to accomplish this, the script that handles individual molecular calculations had to be altered so that when a profile is created it also outputs the individual numerical ozone concentrations. Altering this ozone profile with different values simulates the ozone and TEC variability change noted in the

experimental comparison. Instead of generating the ozone portion of the profile, these altered values are instead loaded into the profile. The spectral properties of this altered profile can be compared with the profile generated before ozone was changed. Several different percentage increases in 30 – 50 km ozone were used to examine this effect, and were based on the percentage change seen in the TEC variability and ozone comparison.

The stations selected for this study were chosen for several reasons. The reasoning was based primarily on their latitude, geographic location, and ozone data availability. The NOAA-EPA Brewer Spectrophotometer UV and Ozone Network (NEUBrew) spectrometers consists of six stations scattered across the United States. The stations are located at the Table Mountain Test Facility (TMTF) in Boulder, Colorado, Houston, Texas, the Mountain Research Station in Nederland, Colorado, Bondville, Illinois, Raleigh, North Carolina, and Ft. Peck, Montana. The two Colorado stations are in close proximity to each other, and the Montana and Illinois stations are frequently limited due to weather conditions and/or instrument malfunction. All stations are located in close proximity to a NOAA-operated Continually Operating Reference Station (CORS) site, and deriving a TEC estimate for the same geographic location as these spectrometer sites was not a limiting factor.

The atmospheric profile used in LEEDR was set to the daily average atmosphere for the summer and at Houston Texas. This location was selected due to the presence of a Brewer sensor in addition to the strong semi diurnal tidal contributions that exist at the station's latitude. The relative humidity was set at the default setting of 50%, which only plays a significant role near the surface. It is also necessary to select the number of layers computed in the model run. The number of layers is based on a full 100 km profile so that

when 1000 layers are selected the thickness of each layer is 100 m. This 100 km atmosphere is a limitation coded within LEEDR. The larger the number of layers that is selected, the longer it will take to generate the profile. On the other hand, the larger the number of layers, the better the resolution. Increasing the resolution beyond 100 m has little statistical impact on the output data (Fiorino et al., 2013).

After generating the profile, ozone needs to be altered by the desired amount. In the cases of the studies mentioned in the literature review, ozone increases by roughly 25% between 30 and 50 km in the case of SSW events. This value is consistent with the short-term ozone variations that are observed later in this study, in addition to long-term variations, which can approach 50%. Increasing the ozone beyond 50% may be useful for demonstrating the radiative effects of ozone on the atmosphere, but would not be a realistic portrayal of stratospheric ozone changes. Because 30 – 50 km is the region primarily responsible for thermal tides, these altitudes will be the focus for the ozone increase.

3.3 Initial Raw TEC Data Collection (CORS)

The National Geodetic Survey (NGS) is a subsidiary of NOAA, and observes a collection of CORS sites. These reference stations collect Global Navigation Satellite System (GNSS) data, which carry data such as carrier position and range. The purpose of this data is to support meteorology, space weather, and geophysical operations across the continental United States. The data collected at CORS stations is output in a Receiver Independent Exchange Format (RINEX). This raw data must be converted into a different format for analysis. This formatted data must be processed and interpreted to form an

accurate estimate of TEC for the receiver's location. The CORS network is comprised of nearly 2,000 receiving stations that are operated by over 200 different organizations. NGS allows new receiving stations to join the network as long as they meet a number of requirements. A few of these stipulations are that the satellite receiver must be dual frequency, track no fewer than 10 satellites, and the data has to be recorded on a 30 second or less interval. Reference sites can also be found in countries all around the world. GNSS data is collected throughout Europe using a separate network of reference stations called the EUREF Permanent Network (EPN), and IGS operates reference stations across the globe.

Navigation and ranging data transmitted from satellites to a receiver must be modulated onto a carrier frequency. Having two or more frequencies transmitted from one satellite enables the ionospheric delay error to be directly calculated. CORS data collected from satellites are characterized as L1, L2, L2C, and L5 data. The L1 frequency is transmitted at 1575.42 MHz and the L2 frequency is transmitted at 1227.6 MHz. L2C is broadcasted at the same frequency as the L2 signal, but was designed to be easier to track, and it also serves as a redundant signal in case of interference. The L5 frequency is transmitted at 1176.45 MHz, which is an aeronautic band so interference can be more effectively managed. Navigation and ranging data used in conjunction with the information regarding the ionospheric delay can be used to estimate the TEC.

While numerous studies throughout the years have attempted to estimate TEC values through GPS networks, the estimation of TEC for a single ground station is problematic due to several factors. TEC estimation is a product of the interpolation of different satellites and frequencies. Variations in the ionospheric refractive index with

frequency can cause major errors in the group delay and phase advance of GPS observables. Because of this, both satellite bias and inter-frequency receiver bias must be accounted for in order to obtain an accurate TEC estimate.

Inter-frequency bias is theorized to be instrumental in nature and is caused by the delay between the analog hardware of the satellite and receiver. Based on this assumption, the inter-frequency bias is modeled as a function of temperature and the instrumentation. One of the models for computing this bias is called IONOLAB, which was developed by the ionospheric research laboratory. IONOLAB computes receiver bias at an individual station by comparing the range and calculated VTEC derived from GPS satellites (Arikan et al., 2008). The bias values obtained by IONOLAB are comparable to daily and monthly estimates derived at available International GNSS Service (IGS) centers (Arikan et al., 2008).

Estimating TEC from a RINEX formatted data file starts with pre-processing of the data, is followed by the actual computation of the TEC, and is completed when the data is presented to the user in a useful format. STEC is the number of electrons per ray path, and is computed in a 30-second time resolution for every satellite. In the actual computation, the VTEC is derived from STEC through the use of a mapping function for every position of the satellites (Sridharan et al. 2013). This mapping function uses the satellite and receiver location to describe the arc path between the two. GPS satellites orbit the Earth at around 20,000 km which means that TEC values estimated form this orbit characterize both the plasmasphere and ionosphere.

3.4 TEC Data Processing and Calculation

Due to effects of the ionosphere on communications, navigation, guidance, and remote sensing, determining the TEC has been a major focus of this study. Ground and space systems measuring TEC are not only limited in space and time, but they are also expensive to maintain and operate. Dual-frequency GPS receivers are a cost effective alternative for estimating TEC. Because of their high orbit, GPS satellites orbit are a long-established method for characterizing the variability of the ionosphere. TEC has been measured from GPS recordings and networks for more than two decades, but there are several inherent problems. Among these problems are the process of calculating satellite and receiver bias and combining TEC measurements from different satellites (Sezen et al., 2013). IONOLAB computes a TEC estimate while solving these issues.

In order to compute estimates of the TEC, IONOLAB uses a method called Reg-Est. The Reg-Est method was first introduced in 2003, and provides reliable TEC estimates for both disturbed and quiet ionospheric conditions. This method is applicable to stations at all latitudes. There has been a thorough comparison of Reg-Est with the Global Ionospheric Map (GIM) TEC from various IGS stations and empirical ionospheric models. Reg-Est TEC estimates have been found to closely match IGS TEC, and closely match results found by the Jet Propulsion Laboratory (JPL) and the Center for Orbit Determination in Europe (Sezen et al., 2013).

The calculation of IONOLAB-TEC is based on preprocessed RINEX files and uses satellite and receiver bias values as well as satellite and receiver location. By combining the receiver bias and computed phase delay values, IONOLAB calculates the STEC and using a mapping function, these values are converted into a VTEC. The VTEC

data from each satellite is combined in a least squares sense and implements a weighting function to adjust for multipath effects for satellites with low elevation angles (Sezen et al., 2013). The multipath adjustment is necessary because data from satellites with a low elevation angle are prone to error because they are more likely to pick up atmospheric noise as well as signal fades.

One of the largest errors in computing TEC from RINEX files stems from cycle slips, which lead to a loss of data. If for some reason there is a data gap in the RINEX file, the missing data undergoes an interpolation routing based on the C-spline of the data gap (Sezen et al., 2013). As long as the duration of missing data is less than 15 minutes with a difference in TEC of less than three TECU, the missing data is interpolated and the data gap is automatically filled. If the data gap is longer than this period, it is designated with an error code.

3.5 Ozone Data Processing (NEUBrew)

Obtaining accurate ozone measurements for the upper stratosphere is a difficult problem. While direct measurements might seem like the obvious solution, ozonesondes only measure ozone up to the point that the balloons burst, which is at around 35 km. The peak tidal heating due to ozone occurs well above this altitude, which rules out ozonesondes for use in this study. However, estimates above this level are obtainable using certain techniques such as the Umkehr method. The Umkehr measurement system was first discovered when Götz noticed that ratio of zenith sky radiances of two wavelengths in the UV, one weakly and one strongly absorbed by ozone, grow with increasing solar zenith angles but plummet as the zenith angle gets close to 90 degrees

(Petropavlovskikh et al., 2011). This is called the Umkehr effect, and was realized to contain information regarding the distribution of ozone in the stratosphere.

The Umkehr method constructs ozone profiles up to 50 km, which is well past the limit of ozonesondes and covers the altitudes in which significant contributions of ozone heating occur. This method is achieved though measuring the intensity ratio of sky-scattered sunlight at a pair of UV wavelengths at solar zenith angles above 70 degrees. This method was discovered in the 1930s and was put into practice beginning in the 1960s at several sites in Australia (Petropavlovskikh et al., 2011). This effect was realized to contain information regarding the distribution of ozone in the stratosphere. Umkehr measurements are taken at sunrise and sunset when solar zenith angles are between 90 to 70 degrees and 70 to 90 degrees, respectively (Petropavlovskikh et al., 2005). This estimate is better used for long-term trends in atmospheric ozone and can be noisy when monitoring short-term variations.

The instruments used to collect the data are Mark IV (MKIV) Brewers, which are devices operated by NEUBrew. Brewer spectrometers came into service in 1982 with the intention to rectify flaws inherent to Dobson spectrometers. In particular, the Brewer sought to eliminate the “optical wedge”, reduce measurement noise, and improve low zenith angle accuracy all in an automatically operated network. The MKIV Brewer added new measurement capabilities such as a spectrally resolving UV radiation. These instruments undergo regular calibration, and measurements undergo post correction every 2 years. Data collected by the spectrometers is continually compared with other measurement sources such as ozonesondes, LIDAR, microwave, and satellites.

Brewer spectrophotometers construct ozone profiles by performing calculations based on the solar zenith angle (SZA). The Brewer spectrometer takes zenith sky measurements by recording intensities of polarized zenith-sky light at five wavelengths nearly simultaneously at two partly overlapping bands, and the resulting Umkehr value is calculated using equation 7. N_{SZA} is an Umkehr value which is measured when the sun is at a particular SZA. F_{SZA} is an Umkehr measurement at the nominal zenith angle, where L2 is the longer (~310 nm) and L1 the shorter wavelength (326 nm) channel. These wavelengths used to measure ozone are in the UV spectrum and are attenuated by cloud-cover, which will limit the data's accuracy. F_0 is an Umkehr measurement taken at the highest solar zenith angle. In this equation, F_{SZA} is intended to simulate measured irradiance. I_{SZA} is the zenith sky radiance that is normalized to the top of the atmosphere. K is an instrumental constant, and ETC is an extra-terrestrial constant (Petropavlovskikh et al., 2011).

$$N_{SZA} = \log\left(\frac{F_{SZA}^{L2}}{F_{SZA}^{L1}}\right) - \log\left(\frac{F_0^{L2}}{F_0^{L1}}\right) \quad (7)$$

$$F_{SZA} = I_{SZA} \times K * ETC \quad (8)$$

Ozone measurements are sampled approximately 50 times while the sun's zenith angle is between 90 and 70 degrees. On average, AM ozone profiles are measured for 2 hours starting at sunrise. PM ozone profiles are measured starting at around 2 hours before sunset and last until sunset. The time and period it takes for the sun to pass from the horizon to 70 degrees from the zenith depends on the time of year and location of the station. The associated morning and sunset TEC values were adjusted every ten days

based on this information. This TEC data was then averaged for each corresponding period of time so that a single ozone value corresponds to a single TEC value.

Brewer spectrometers have several faults. The solar zenith angle requirement limits the duration in which ozone can be observed, and since the instrument is solar irradiance based, data collection requires mostly clear skies. In addition, out-of-band (OOB) light can cause impacts to direct-sun, UV, and zenith measurements. OOB light can affect the low intensity spectrum of solar light, which is not fully removed by the optical bandpass of the spectrometer. This additional light source contributes to the photon count with the biggest impact coming from wavelengths just outside the bandpass. NEUBrew runs a quality control algorithm checking for these conditions, and considers the deviations between profiles. Many of the calculated ozone profiles do not pass these criteria, and this data was not used for analysis purposes. This leads to periods of missing data for all Brewer stations. The Brewer data is processed using a retrieval algorithm called the UMK04. The UMK04 divides the atmosphere into 61 layers using an averaging kernel to further divide the standard 4.8 km Umkehr layer into 4 sections. The UMK04 is based on an estimation technique with a purpose of moving away from theory, and moving using more data than the previous model (Petropavlovskikh et al., 2005).

The goal of the analysis was to show the relationship between the 30 – 50 km ozone values and TEC variability. Ozone is only measured by Brewer spectrometers when the solar zenith angle is between 90 and 70 degrees. These angles occur both during sunrise and sunset. TEC values just after sunrise are not typically at the diurnal minimum. In addition, TEC values taken just before sunset are not a true maximum; however, taking the difference between the two gives a diurnal variation that corresponds to the morning

and evening ozone profiles. Their relationship can then be examined by correlating the two and comparing morning and evening ozone to the diurnal TEC variation. While TEC can be derived for any time of the day, in order to achieve a more direct comparison, TEC will be averaged for the same time-duration in which ozone is sampled.

3.5 Methodology Summary

This chapter detailed the various models and data sources used to correlate stratospheric ozone and TEC variability in addition to using radiative transfer models to observe the effect that changes in stratospheric ozone have on radiation. TEC estimates were derived from the IONOLAB model, which uses satellite data computed at CORS sites. Stratospheric ozone profiles are calculated using BREWER spectrometers. NEUBrew consists of the system of Brewer spectrometers that record this data, which is then converted into usable ozone profiles. The pairing of NEUBrew and IONOLAB enable the comparison of TEC variability and stratospheric ozone. The radiative transfer model used in this study is called LEEDR, and allows for altering individual atmospheric absorbers. This program could be used to investigate how stratospheric changes in ozone effect the path radiance at a selected location. Combining these models and data sources led to the creation of a long-term comparison between stratospheric ozone changes and TEC variability.

IV. Analysis and Results

4.1 Overview

This section will discuss the data that results from calculating the correlation between stratospheric ozone and TEC variation. TEC and stratospheric ozone data were collected at three different stations. The first is located in Houston, Texas (station identifier NETP). The second is located in Colorado Springs, Colorado (station identifier TMTFCO). The last station is located in Raleigh, North Carolina (station identifier NCRD). Data from NETP and TMTFCO were collected from Jan 01 to Aug 31, 2016. Due to the limitations associated with the Brewer Spectrometers, data from NCRD was collected for the same months, but for 2013. By using data for these three stations, it is possible to gain insight regarding effects due to latitude and point in the solar cycle. The latitudes that are sampled range between 30N and 40N. The solar cycle range from just after the last solar maximum until near the current solar minimum. This data will be presented through time-series plots, scatterplots, and numerically through a table. This section will also cover the radiative changes calculated in LEEDR due to realistic fluctuations in stratospheric ozone.

4.2 TEC Variability and Stratospheric Ozone Comparison

This is an overview for the basic structure of the time series plots. The title describes the altitude-levels of stratospheric ozone used in the correlation. The x-axis is the day of the year in which ozone and TEC were estimated. The major y-axis on the left describes the morning to evening diurnal variation in TEC in the units of TECU. The timing was used to line up with the measurements of ozone recorded by Brewer

spectrometers. More specifically, this is the difference between the TEC measured at sunset when the zenith angles are between 70–90 degrees and the TEC measured at sunrise when the zenith angles are between 90–70 degrees. The minor y-axis on the right includes the average ozone from the selected stratospheric altitude-levels and is measured in 10^{11} molecules per cubic centimeter. The orange line includes the time series data for the diurnal change in TEC. The blue line includes the time series data for the Brewer averaged ozone. The time series charts were constructed for both morning and evening stratospheric ozone estimates. Both estimates are plotted as a three-day moving average. The reasoning for the moving average is that there are data-gaps caused when the stratospheric ozone measured on the Brewer spectrometers does not pass quality control. There are instances when these data-gaps can last for a week, and using a moving average helps to bridge this gap.

Figure 2 includes morning time-series plot for NETP. Stratospheric ozone and TEC variation visually trend together at this time, and the altitude in which the strongest relationship was observed was from 27–45 km. This altitude band closely matches levels which experience substantial heating due to stratospheric ozone. Both stratospheric ozone and TEC variability rise rapidly from January heading into the beginning of April, when both level-off. In early January, diurnal TEC variations are approximately five TECU, whereas by the beginning of April these variations balloon to an average of ten TECU. The average ozone for the 27–45 km layer also increases by a substantial percentage. Average stratospheric ozone concentrations increase from to 11×10^{11} to 13×10^{11} molecules per cubic centimeter during this length of time. Within Figure 3, the PM time-

series plot shows a similar trend, both rise rapidly from January into early April when both level off.

While stratospheric ozone and TEC variability follow the same general trends, variations are obvious on specific dates. One specific instance occurs in Figure 2 from February 17 to March 1, when TEC variability spikes upwards and then downwards while stratospheric ozone observes only minor changes. This event in particular can likely be attributed to a large number of solar flares and geomagnetic storming observed from 16 – 18 February, when AP indexes reached above 50 several days in a row. Another deviation occurred on May 7th when AP values approached 100 associated with strong geomagnetic storming. Changes like these can often be attributed to similar events and drivers of TEC variability such as the solar flux and geomagnetic activity and even cases of instrument error. The duration of these spike are also increased due to using a three day average to fill in data gaps.

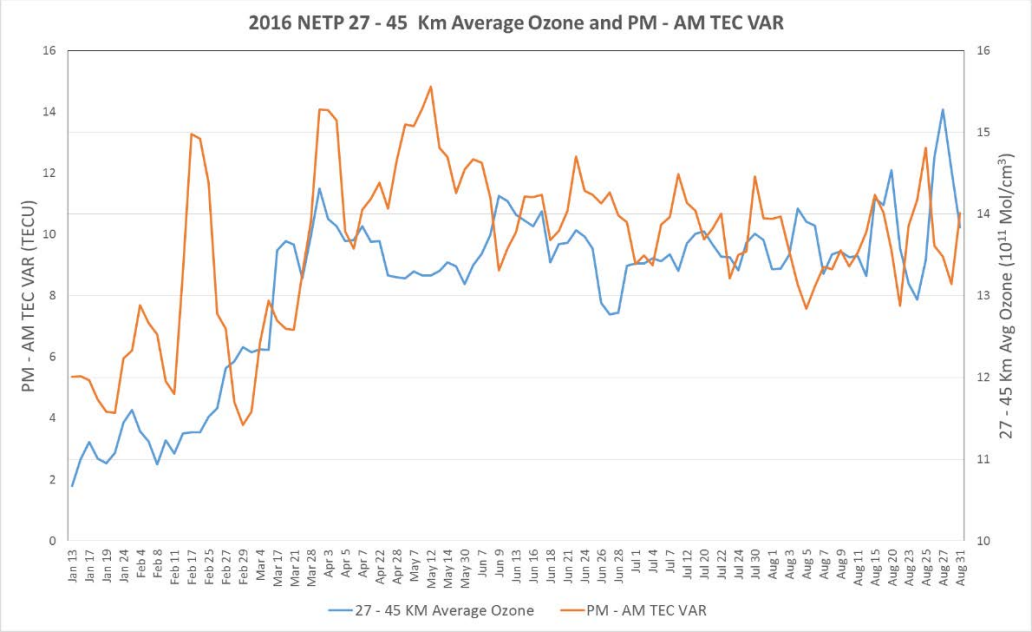

Figure 2: NETP AM Time Series
Houston, Texas, station ID (NETP) AM Time Series. PM – AM TEC difference (Orange) and AM measured 27 – 45 km Avg Ozone (Blue) plotted by date.

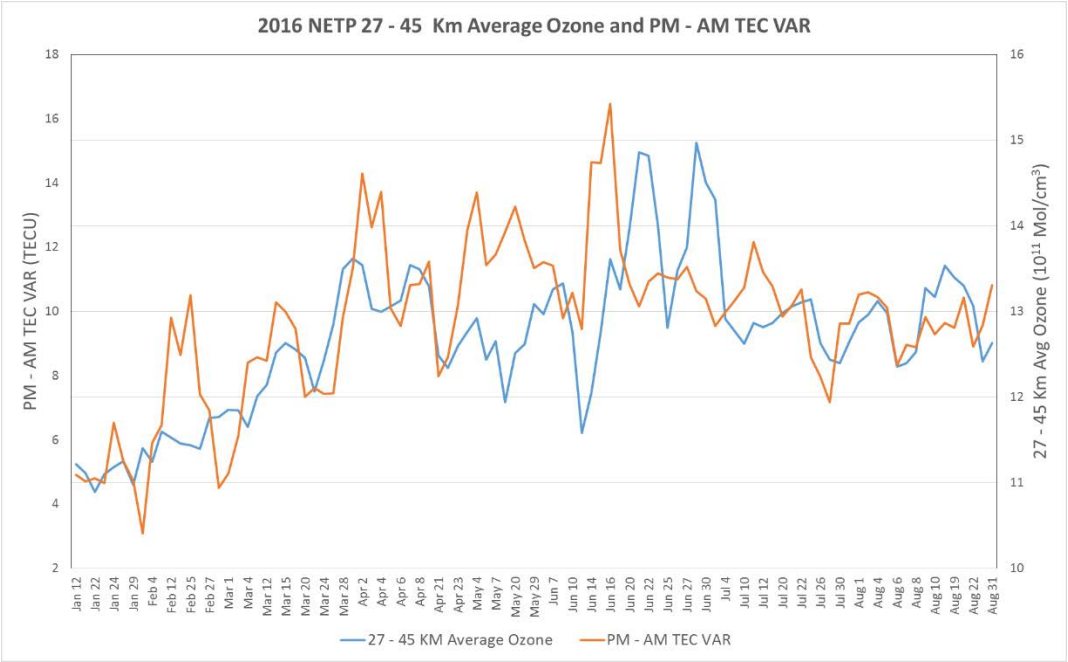

Figure 3: NETP PM Time Series
Houston, Texas, station ID (NETP) PM Time Series. PM – AM TEC difference (Orange) and PM measured 27 – 45 km Avg Ozone (Blue) plotted by date.

In Figures 4 and 5, the AM and PM time series for TMTFCO show only slight increases in TEC variability and stratospheric ozone concentrations for the first several months of 2016. The trends in TEC variability and ozone are inconsistent with the data measured at Houston primarily due to ozone's data availability. When several days are missing during a period of high geomagnetic activity, an associated increase in TEC variability will also be missing. An example of this problem can be seen in a spike in March for the AM time series plot. On March 6th, geomagnetic storming conditions resulted in an AP index of 90. This initiates a spike in TEC variability. Both data sets begin to actually decrease slighting starting in mid-April. TEC variability in general was lower for this station compared to NETP and follows a different trend. The strongest relationship between the two data sets was observed from 35 – 47 km, and begins to fall off as the minimum altitude is lowered. Stratospheric ozone averages around 4×10^{11} molecules per cubic cm, and falls down to 3.4×10^{11} molecules per cubic cm by May. Overall, there is a much closer relationship for the AM TEC variability comparison with stratospheric ozone than the PM comparison. One particular dissimilarity seen in Figure 5 occurs when there is a general rebound in TEC variability in June that is not captured by stratospheric ozone concentrations.

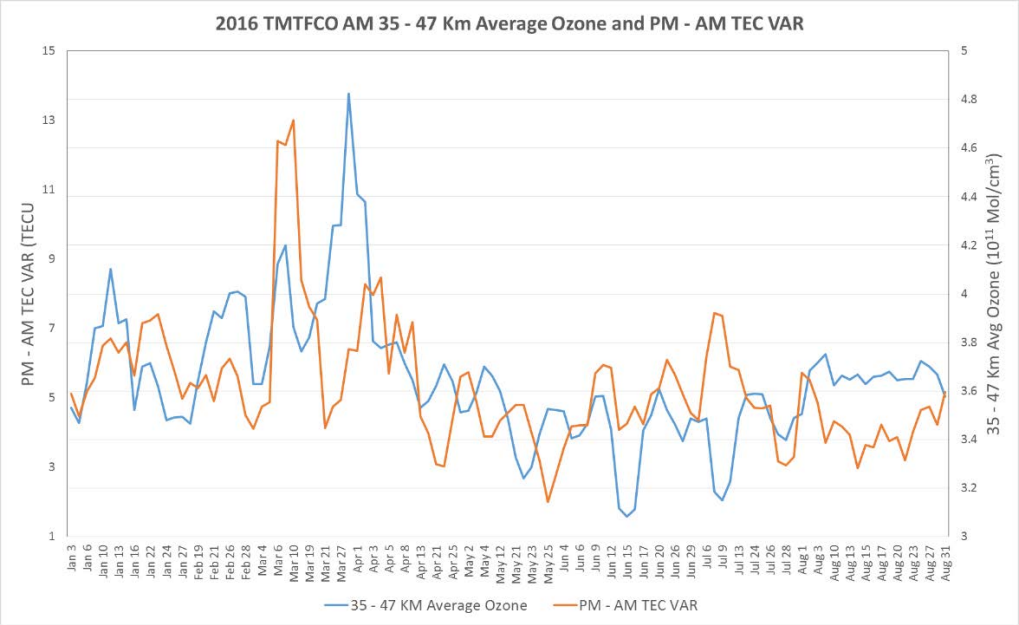

Figure 4: TMTFCO AM Time Series
Colorado Springs, Colorado, station ID (TMTFCO) AM Time Series. PM – AM TEC difference (Orange) and PM measured 35 – 47 km Avg Ozone (Blue) plotted by date.

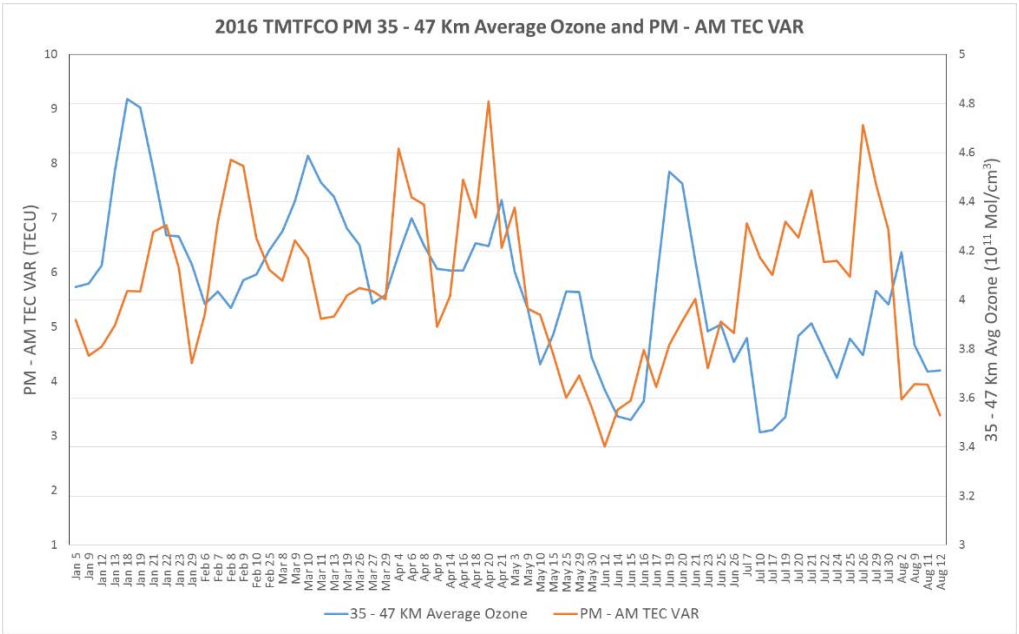

Figure 5: TMTFCO PM Time Series
Colorado Springs, Colorado, station ID (TMTFCO) PM Time Series. PM – AM TEC difference (Orange) and PM measured 35 – 47 km Avg Ozone (Blue) plotted by date.

Before detailing the time series plot for NCRD, consider the altitude for which the data was derived. The most substantial relationship for this station is achieved from 19–39 km, which is significantly below the other two stations. Statistically noteworthy contributions of thermal tides due to ozone occur primarily from 30 – 50 km, so some of this contribution is coming from below that level. Data for this station regarding the general trend of stratospheric ozone and TEC variability trails off considerably above these altitudes. The data for NCRD is also different from the other two stations for other reasons. For one, there is about a quarter less data points for NCRD than either of the other stations. In addition, data for this station was collected for 2013 due to issues with the Brewer sensor resulting in the loss of data for the following years.

For NCRD, Figure 6 shows that the AM stratospheric ozone comparison with TEC variability follows the same general trend. For the AM comparison, both increase significantly from the beginning of January into the middle of April where they begin to level off. As seen in Figure 7, the PM stratospheric ozone comparison with TEC variability association is still observable, however; it is much less apparent. While stratospheric ozone concentrations gradually increase during the course of the year, TEC variations flatten out towards the beginning of April and continue to oscillate at nearly the same values during the rest of the year.

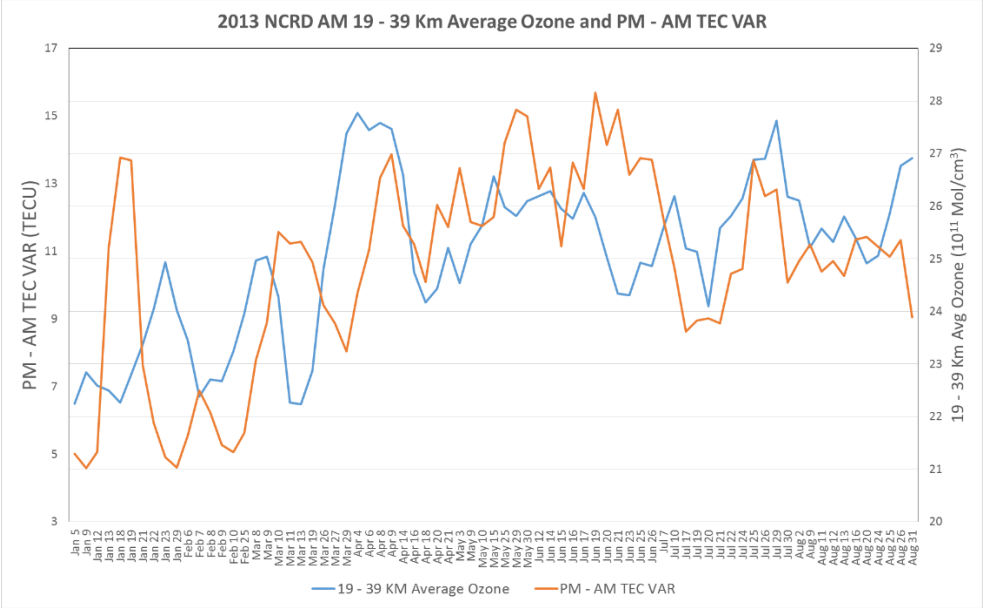

Figure 6: NCRD AM Time Series

Raleigh, North Carolina, station ID (NCRD) AM Time Series. PM – AM TEC difference (Orange) and AM measured 19 – 39 km Avg Ozone (Blue) plotted by date.

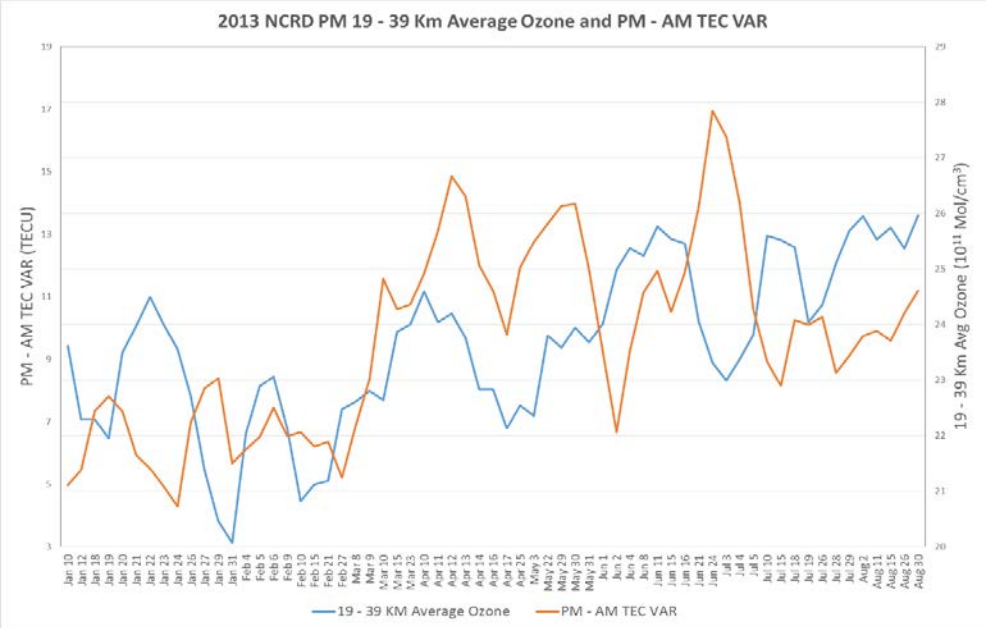

Figure 7: NCRD PM Time Series

Raleigh, North Carolina, station ID (NCRD) PM Time Series. PM – AM TEC difference (Orange) and PM measured 19 – 39 km Avg Ozone (Blue) plotted by date.

4.3 Scatterplots and Correlation Table

Scatterplots generated from this research consist of directly correlating pairs of average stratospheric ozone to TEC variability. As in the case of the time series charts, both stratospheric ozone and TEC variability are converted into a three day moving average before being plotted. The title describes the relative time (AM or PM) and altitude-levels of stratospheric ozone used in the correlation. The x-axis consists of the average stratospheric ozone at the selected altitude-levels is measured in 10^{11} molecules per cubic centimeter. The y-axis is the diurnal difference between PM and AM TEC, and has units in TECU. In addition, a linear trend line has been fitted to illustrate the positive correlation and general trend of the data. Other fit-methods were applied, but there wasn't a singular method that better captured the correlation than a linear fit line. These graphs illustrate the same concept as the time-series plots; however, they are additive in that they present the correlation in a more direct manner.

Again starting with NETP in Figure 8, the AM comparison revealed moderately strong positive correlation between stratospheric ozone from 27–45 km and the diurnal TEC variation. As seen in Figure 9, the PM comparison also shows moderately strong correlation, and is slightly more continuous than the AM data. A Pearson product moment correlation was calculated for these data pairs using a process that will be described later in this section. Between the two, the AM and PM data correlation coefficients are .5278 and .5915 respectively as indicated by Table 1. By considering the equations of the linear trend of these graphs, it is possible to make an estimate of either TEC variability or stratospheric ozone based on unknown parameter. There is also evidence that after the stratospheric ozone concentrations reach around 14×10^{11}

molecules/cm^3, the positive trend levels out and there is no longer a substantial increase in daily TEC variability. This flattening-out trend was evidenced in both the AM and PM comparisons. This indicates that increasing stratospheric ozone at these altitudes has diminishing effects on thermal tides at a certain point.

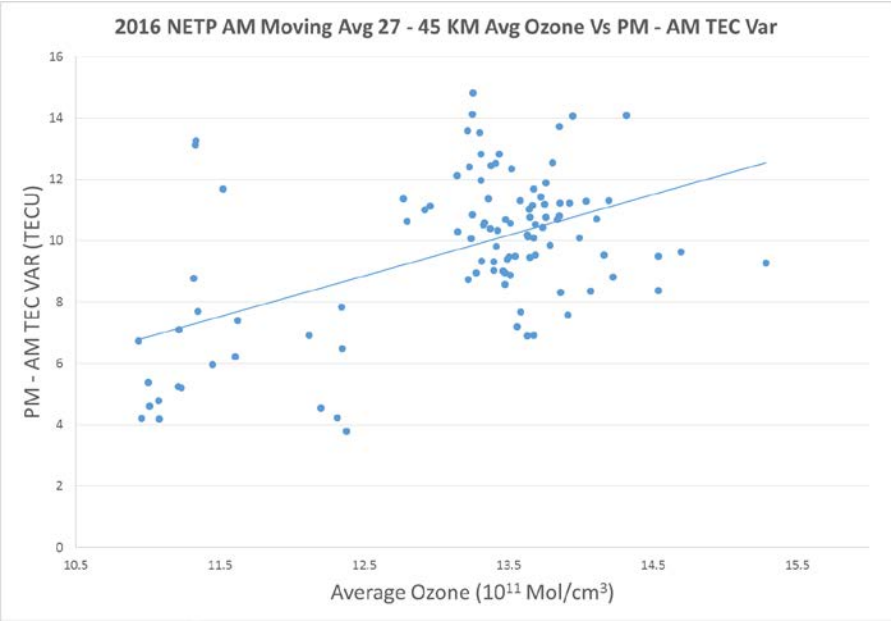

Figure 8: NETP AM Comparison
NETP AM Stratospheric Ozone Vs TEC Var. Linear trend line in blue dots.

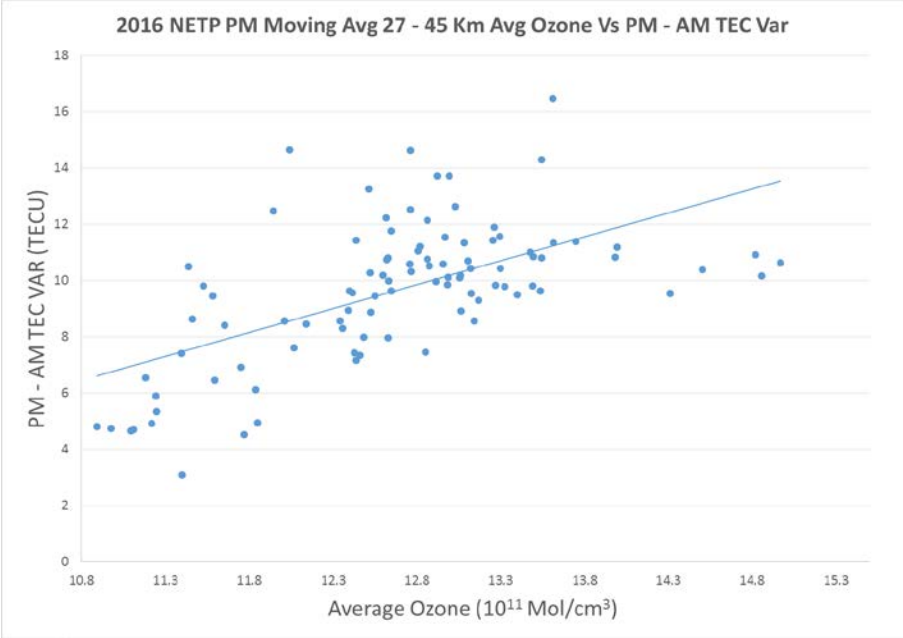

Figure 9: NETP PM Comparison
NETP PM Stratospheric Ozone Vs TEC Var. Linear trend line in blue dots.

At TMTFCO, the scatterplot follows a weak-to-moderate linear correlation pattern for the AM comparison shown in Figure 10. The PM correlation seen in Figure 11 is much weaker, yet still shows a positive trend. The correlation values for these times are .3714 and .2065 respectively as indicated in Table 1. Similar to TMTFCO, scatterplot data for NCRD shows a weak-to-moderate linear correlation for the AM comparison with TEC variation as seen in Figure 12. Average ozone values are much higher at NCRD because of the lower altitude of the layer that was correlated. Again, the PM variation is weak but still positively correlated as shown in Figure 13. Respectively, the correlation values for NCRD at these times are .4235 and .1899 as indicated in Table 1. Neither station shows correlations as strong as what was observed at NETP.

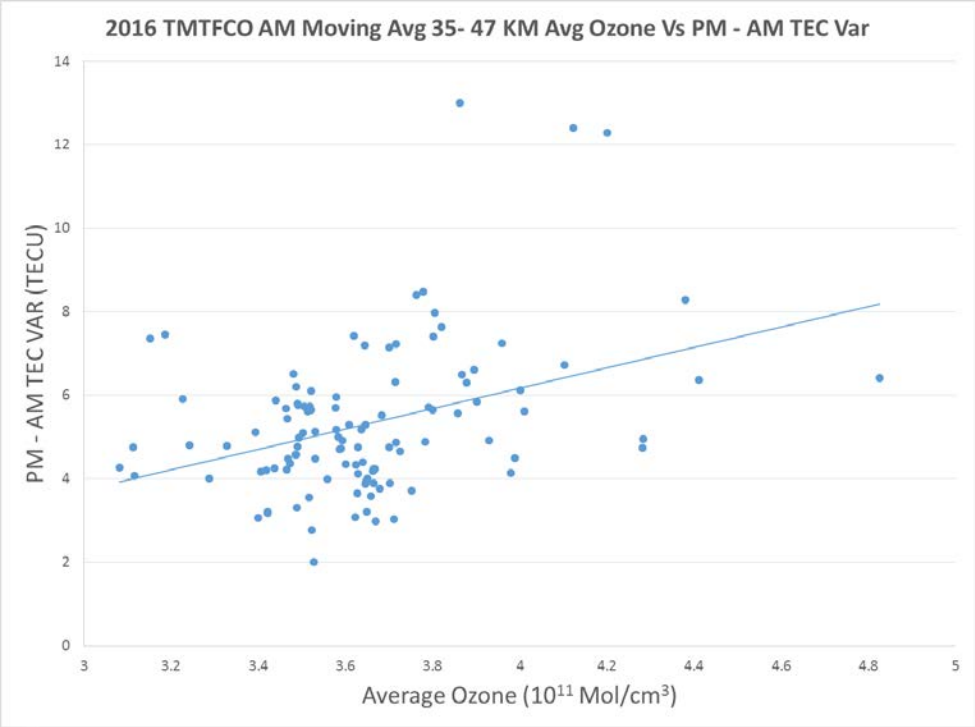

Figure 10: TMTFCO AM Comparison
TMTFCO AM Stratospheric Ozone Vs TEC Var. Linear trend line in blue dots.

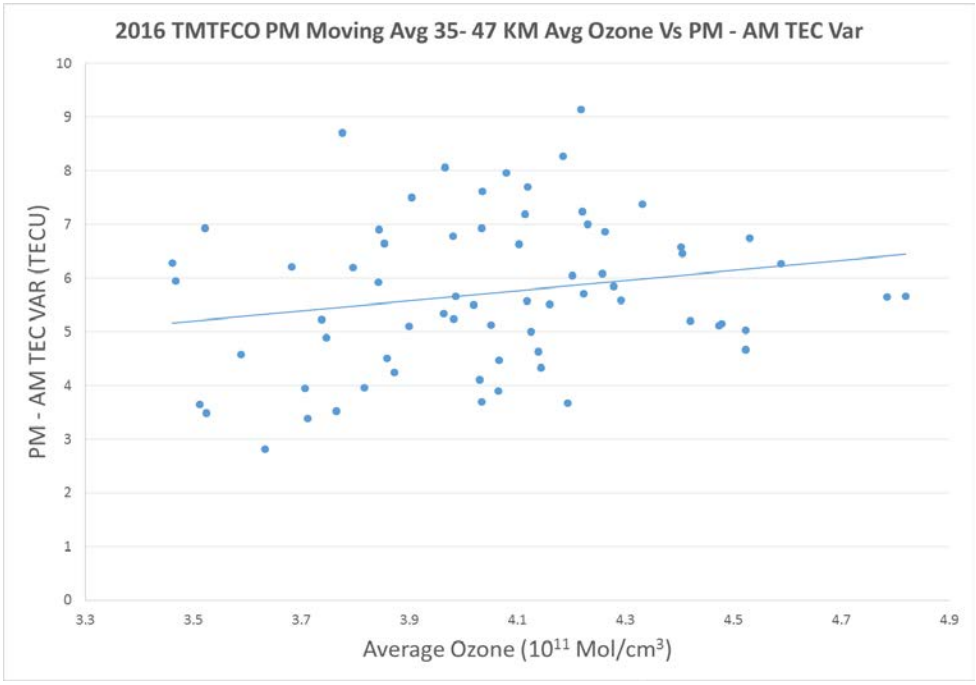

Figure 11: TMTFCO PM Comparison
TMTFCO PM Stratospheric Ozone Vs TEC Var. Linear trend line in blue dots.

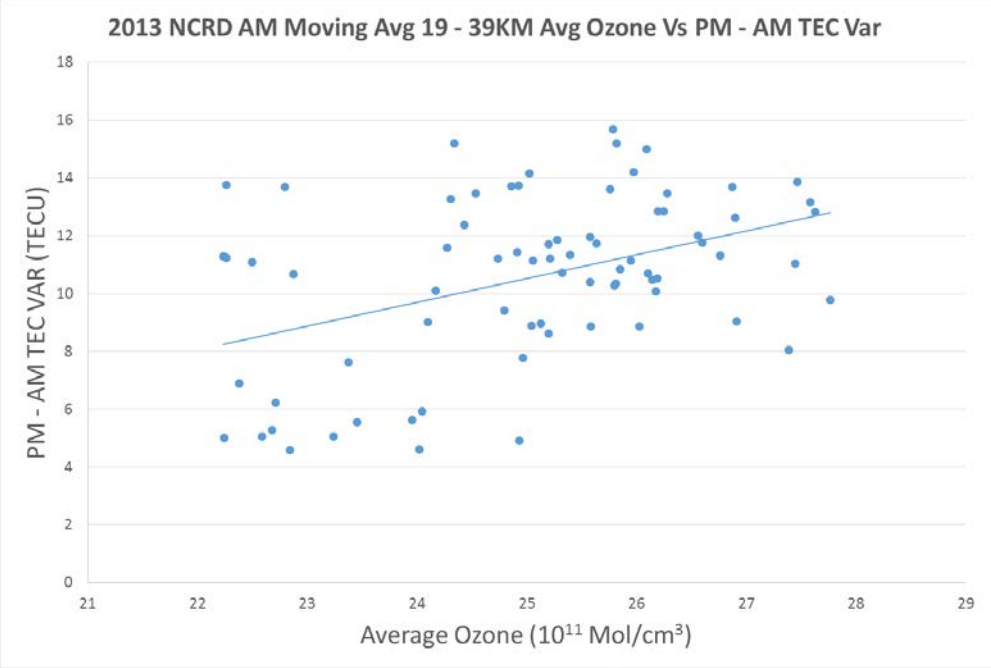

Figure 12: NCRD AM Comparison
NCRD AM Stratospheric Ozone Vs TEC Var. Linear trend line in blue dots.

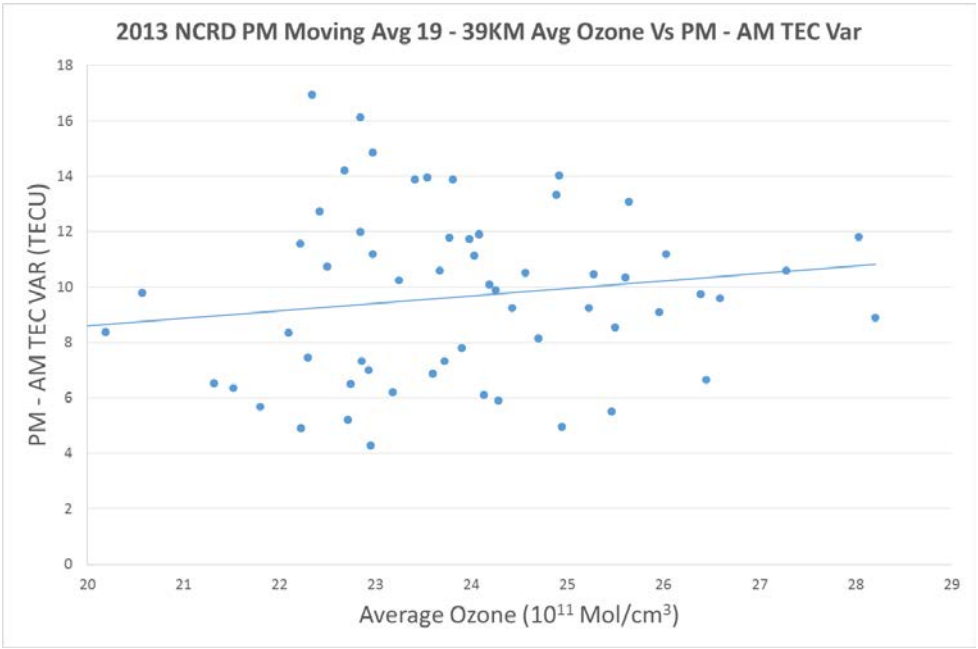

Figure 13: NCRD PM Comparison
NCRD PM Stratospheric Ozone Vs TEC Var. Linear trend line in blue dots.

Table 1. Stratospheric Ozone and TEC Var Correlation by Station

Station ID	Altitude (km)	Ozone Measurment Time	# Ozone Observations	Correlation (R) w/ TEC Var
NETP	27-45	AM	107	0.5278
NETP	27-45	PM	99	0.5915
TMTFCO	35-47	AM	113	0.3714
TMTFCO	35-47	PM	71	0.2065
NCRD	19-39	AM	77	0.4235
NCRD	19-39	PM	65	0.1899

As stratospheric ozone has not been correlated with TEC variability for an extended range of time, there is not a set standard in measuring this correlation. This correlation would need to take into account that migrating tides are only one of the drivers of ionospheric TEC variability, the intrinsic errors of estimating both TEC and stratospheric ozone, and data availability of stratospheric ozone. Because of these limiting factors, correlation was calculated using the Pearson product moment correlation coefficient. This number is usually designated with the letter "R" in statistical research. The correlation coefficient for two arrays of values, a and b, is given by the following formula where $\bar{a}$ and $\bar{b}$ are the sample means of the two arrays of values. The Pearson method is used to demonstrate linear correlation between two variables, and describes how well the data can be fit to a line. A correlation coefficient of one is when two variables are perfectly correlated, a zero describes when two variables show no discernable correlation, and a negative one indicates that two variables share a perfectly negative linear correlation. This negative correlation would indicate that increasing one variable leads to a decrease in the other.

$$R \propto \text{Correlation} = (\sum(a-\bar{a}) * (b-\bar{b}))/\sqrt{(\sum(a-\bar{a})^2)\sum(b-\bar{b})^2} \quad (9)$$

There is an apparent correlation between upper stratospheric ozone and the diurnal change in TEC, but that alone does not confirm a statistically significant relationship. In order to provide evidence of this relationship, it is useful to consider the odds that this data is correlated by random chance. Given a 100 pairs of data points, in order to achieve a 99% confidence interval that data is statistically related, there needs to be a correlation coefficient of .254 or higher between them. This means that for 100 pairs of random data, they would only demonstrates a correlation of .254 or higher just 1% of the time. For a 90% confidence interval, the correlation coefficient just has to be .164 or higher (University of Connecticut, 2015). For the Houston station, this condition is met for both the AM and PM measurements. For the Colorado and Raleigh stations, the AM correlations are well within a 99% confidence interval and the PM comparison remain around the 90% confidence interval. The next section will concern the difference in correlation between the three stations.

Ozone is a secondary source of TEC variation and it has been estimated that planetary waves only account for around 20% of overall TEC variation. Considering this, correlation values between stratospheric ozone and TEC variability should not exceptionally high. In fact, the high correlation observed at NETP provides evidence that the lower atmosphere is a strong driver of TEC variability. The fact that the data is correlated over nearly a full year of data provides further evidence that the stratosphere and ionosphere are coupled.

The majority of research exploring thermal tides has a narrow focus, and only pertains to SSW events at low latitudes. Because there is a semidiurnal migrating tide maxima at lower latitudes, and since stratospheric ozone and TEC variation has been

shown to increase during SSW events, previous research has come to the conclusion that the two are linked. By expanding the research to different latitudes and longer periods of time, this research is aimed beyond event based increases of migrating tides and the related increase in stratospheric ozone. Instead, by investigating ozone's relationship with TEC variation over a longer period of time, it is possible to estimate the direct effect that a change in ozone has on TEC variation.

4.4 Radiative Transfer Calculations (LEEDR)

The other branch of this research involves using LEEDR to investigate stratospheric ozone's radiative effects. Adjusting the stratospheric ozone profile created in LEEDR leads to a significant difference in the calculated path radiance for the both the UV and IR ozone absorption bands. Adding more stratospheric ozone introduces more absorption and lowered path radiance, while reducing stratospheric ozone would have an opposite effect. This change in radiance can be observed not only during the day, but even with backscatter emissions when the sun is below the horizon.

Figure 14 shows the change in the IR ozone absorption band when accounting for a 50% increase in 30–50 km ozone. For this increase in ozone, path radiances are not significantly affected. The reason for this lack of change has to do with the location and climate of the selected site. Because it is near the coast, Houston experiences an especially significant amount of water vapor. This increase in water vapor greatly effects the transmissions along this wavelength band and marginalizes the relative impact of a change in ozone. The difference in path radiances associated with an increase in ozone is

especially difficult to observe between 9.55 and 9.59 µm where ozone is an especially strong absorber, and changes in ozone do not affect the transmission as much.

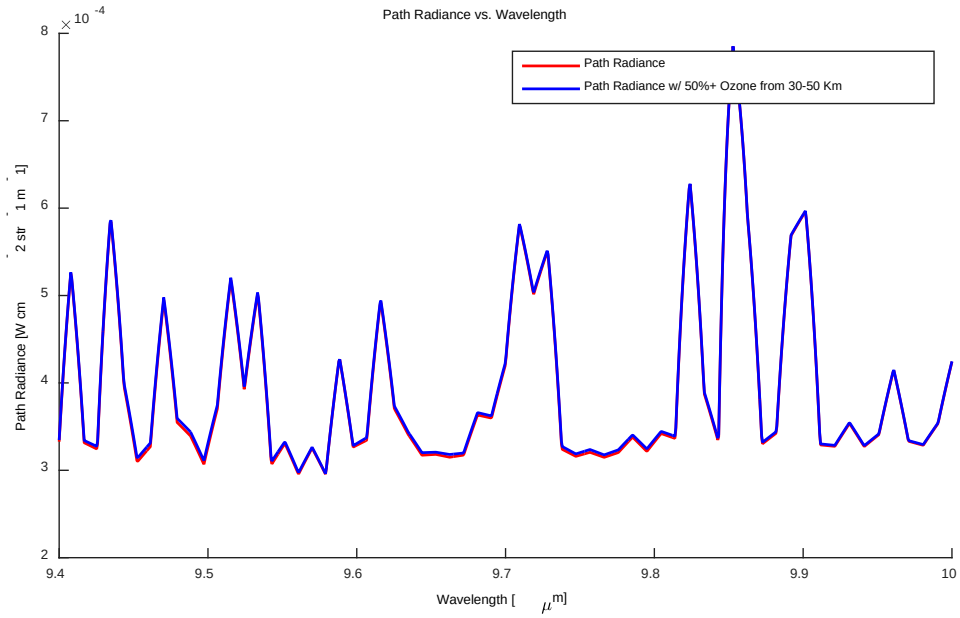

Figure 14: LWIR Downwelling Radiance
Spectral Radiance Change w/ Increased Stratospheric Ozone in the IR band. Zenith angle and azimuth are set to 0 degrees looking up from 1 meter. Unaltered ozone is illustrated in red. Ozone with the 30 – 50 km region increased by 50% is shown in blue. The location of the site is in Houston, Texas at 1400UTC.

Figure 15 illustrates the change in the IR upwelling radiance (i.e. zenith angle equals 180 degrees) when stratospheric ozone is increased by 50%. Radiances in the LWIR are primarily due to emissions, and not backscattering. The increase in ozone results in increased absorption and a decrease in path radiance. Compared to having an azimuth set to 0 degrees, the path radiance for backscatter better illustrates the absorbance of ozone in this wavelength band. The change in stratospheric ozone doesn't have huge impacts on backscatter emissions. The difference in the path radiance after the ozone change is only about 2%. The largest difference as a percentage between the two

path radiances is around 9.5 µm. These comparatively smaller differences in path radiances would make changes in stratospheric ozone harder to detect.

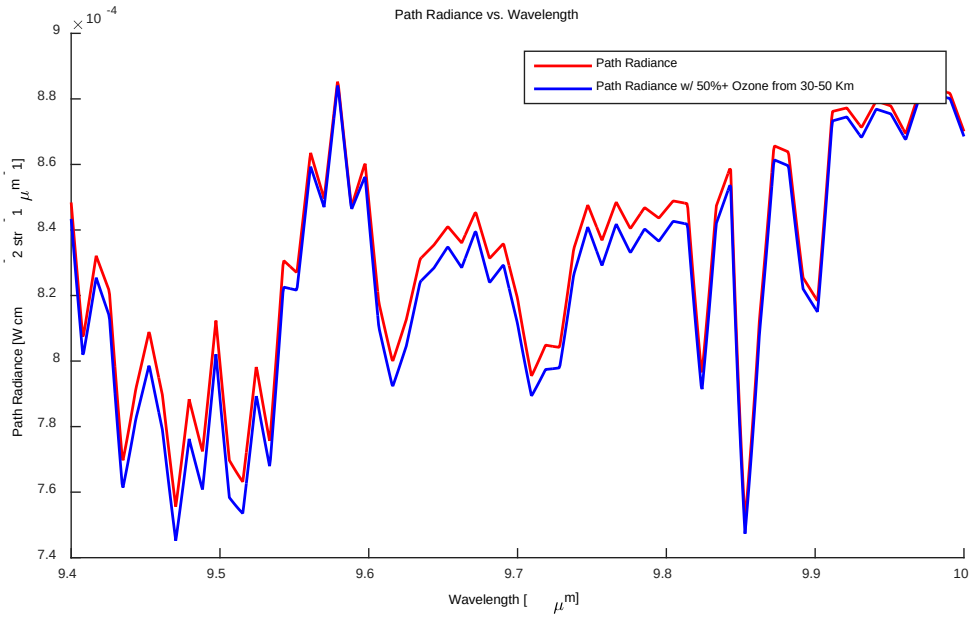

Figure 15: LWIR Upwelling Path Radiance
Spectral Radiance Change w/ Increased Stratospheric Ozone in the IR band. Zenith angle is set to 180 degrees for backscatter and azimuth is set to 0 degrees looking down from 100 km. Unaltered ozone is illustrated in red. Ozone with the 30 – 50 km region increased by 50% is shown in blue. The location of the site is in Houston, Texas at 1400UTC.

The calculated path radiance for the peak UV ozone absorption band in plotted in Figure 16. Projecting a 50% increase in 30 – 50 km ozone leads to an associated decrease in path radiances by up to 23%. These changes are most easily observable from 30 to 30.5 nm, and mainly at the local absorption maxima. Similar to the IR, an increase in stratospheric ozone also causes increased absorption and a decrease in path radiance. There are some noticeable differences between the changes in path radiances seen in the UV versus the IR. The path radiances for the IR absorption band are consistently observable through the majority of its respective absorption band, whereas differences in

the UV are isolated. In both cases, path radiance differences are substantial enough to be observed using spectrometers. In summary, changes in stratospheric ozone can be given a path radiance observed for these specific wavelength bands.

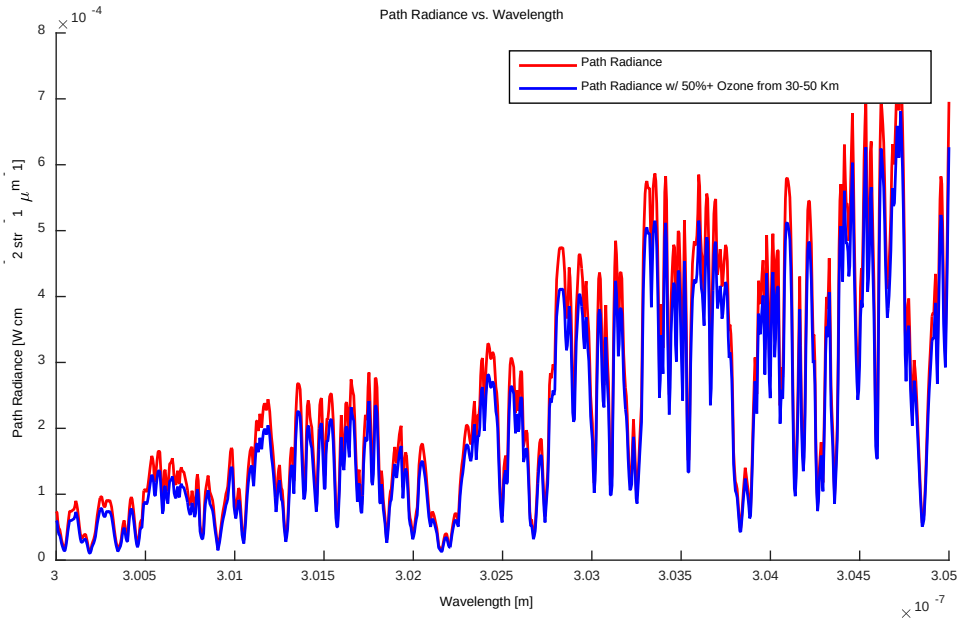

Figure 16: UV Path Radiance
Spectral Radiance Change w/ Increased Stratospheric Ozone in the UV band. Zenith angle and azimuth are set to 0 degrees looking up from 1 meter. Unaltered ozone is illustrated in red. Ozone with the 30 – 50 km region increased by 50% is shown in blue. The location of the site is in Houston, Texas at 1400UTC.

Backscatter path radiances in the UV ozone absorption band are also significantly changed by stratospheric ozone differences. Again, the backscatter path radiances for the UV absorption band are very similar to the path calculated for when the sun is overhead except for the order of magnitude. The increase in ozone still results in increased absorption in the stratosphere which a decrease in path radiance through the layer. In this instance, a 50% increase in 30 – 50 km ozone leads to an associated decrease in path radiances by up to 25%. These percentage differences are larger near 30 to 30.5 nm.

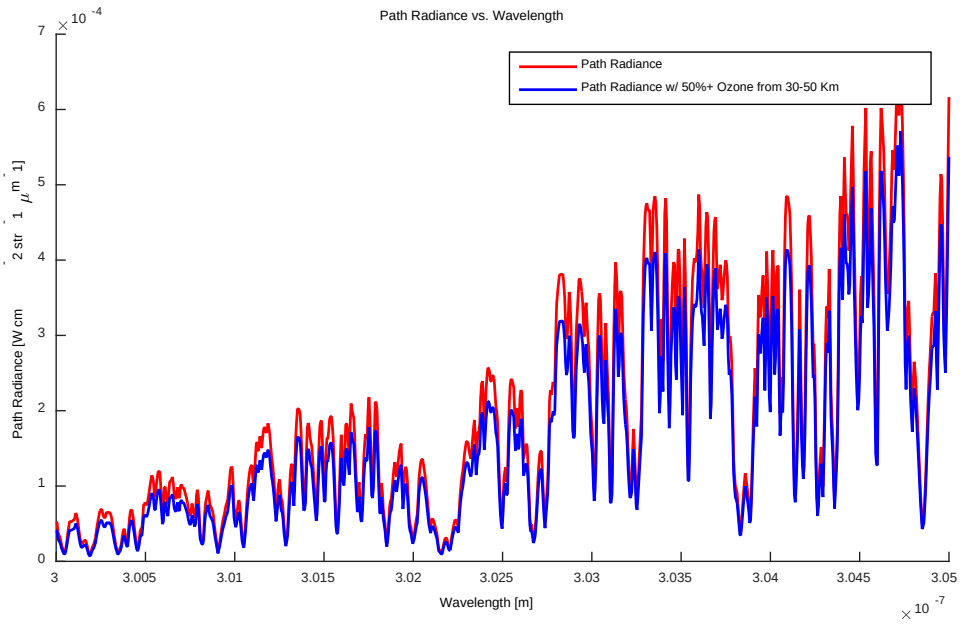

Figure 17: UV Backscatter Path Radiance
Spectral Radiance Change w/ Increased Stratospheric Ozone in the UV band. Zenith angle is set to 180 degrees for backscatter and azimuth is set to 0 degrees looking down from 100 km. Unaltered ozone is illustrated in red. Ozone with the 30 – 50 km region increased by 50% is shown in blue. The location of the site is in Houston, Texas at 1400UTC.

4.5 Summary

The main questions that this research intended to answer is whether there is a direct link between stratospheric ozone and TEC variability, and whether a realistic ozone change can be observed through radiative spectrum analysis. In the first case, there is an apparent link between the two and positive correlations were observed for three different stations. However, variations in this correlation depending on the latitude of the station and year in which the data was collected give rise to other questions which will be addressed in the next chapter. In the second case, realistic increases in stratospheric ozone has an observable effect on the radiative emission spectrum. This is true in both the UV and IR bands, and can even be seen in the backscatter path radiance.

Positive stratospheric ozone correlations with TEC variability were observed at all three stations. However, the strength and altitude levels at which this correlation was observed varied significantly. The strongest correlation was observed at NETP, which has a latitude of approximately 30 degrees. NCRD experienced the weakest correlation when considering ozone at the altitudes in which the peak heating due to ozone should occur. It should be noted that data from this station was collected from 2013 due to limitations of the Brewer spectrometer at that site. Potential reasons for the correlation variability will be outlined in the next section.

LEEDR calculations showed that altering the amount of stratospheric ozone led to significant changes in both the path radiance solar and backscatter emissions. Between IR and UV, these changes were larger for the UV ozone absorption band; however, both could potentially be used to detect fluctuations in stratospheric ozone. The next section will explain how this change in path radiance might be used as a measuring tool for TEC variability and vice versa.

V. Conclusions and Recommendations

5.1 Summary

This study explored the relationship between stratospheric ozone and TEC variability. In doing so, the research addressed two major questions. The first was whether stratospheric ozone could be directly correlated to TEC variability. The second substantiated the possibility that path radiances could be used to observed changes in stratospheric ozone. The following will address how effectively this paper answered these two questions. In addition, this section will concern potential outlets of this research, and other measuring techniques that can account for the inherent weaknesses of ground-based ozone measurement.

While all three stations observed correlation between upper stratospheric ozone and TEC variability, the correlation varied significantly. Compared to the correlation observed at NETP, the correlation at NCRD was comparatively weak for the upper stratosphere, although data collected for that station was taken during a solar maximum. The correlation at TMTFCO was also weak compared to NETP, and this difference can be theorized to result from the difference in latitude between the two stations. Based on the relationship between the three stations, TEC variability and stratospheric ozone correlation shows dependence on both the latitude and point in the solar cycle. In addition, LEEDR showed that fluctuations in stratospheric ozone induce a significant change in both UV and LWIR emissions. Therefore, fluctuations in these emissions could indicate a change in stratospheric ozone, or by association, a change in TEC variability.

5.2 Conclusions of Research

All three stations exhibited a statistically significant correlation between stratospheric ozone and TEC variability; however, the magnitude and altitude of these correlations varied. The NETP Houston site showed the strongest stratospheric ozone to TEC variability relation. To theorize why the correlation at the Houston station was significantly higher than the Colorado or Raleigh stations, it is helpful to recall the tides associated with stratospheric ozone. Migrating tides are associated only with the sun's motion. The tilt of the planet causes uneven incoming solar radiation observed during the various seasons of a year, and the resulting harmonics of these tides have been found to be strongly dependent on latitude as shown by SABER in Figure 1. Houston is more than 10 degrees south of Colorado Springs, which is a significant enough change for the station to experience an increase in the migrating tide. The annual correlation between TEC variability and stratospheric ozone at only three stations may only provide a sampling of this latitudinal dependence. A lack of Brewer stratospheric ozone data was the limiting factor in using other stations to confirm this correlation.

This finding substantiates the thermal tides indicated by SABER, which shows that there is a local maximum of diurnal and semidiurnal migrating tides centered at 30 degrees latitude as seen in Figure 1. Approaching 40 degrees, the diurnal component drops off, and semidiurnal tides should experience more dramatic seasonal variations. This coincides with the stratospheric ozone and TEC variability relationship observed at Raleigh North Carolina (NCRD) and Colorado Springs (TMTCO) stations where the correlation was weaker.

At TMTFCO, the AM and PM correlation between TEC variation and stratospheric ozone fades starting in June, which is when SABER indicates semidiurnal tidal amplitudes are shown to drop as seen in Figure 1. NCRD is further to the south and would not experience this seasonal drop in semidiurnal tides until later. However, this does not explain why correlation at the level of peak stratospheric ozone heating is weaker for NCRD than TMTFCO. The weak upper stratospheric correlation seen at NCRD can be explained in part due to the year in which the data was observed. The data from this station was collected in 2013, which coincides with the last solar maximum. Data from the other two stations were collected in 2016, which is more than halfway to the next solar minima. It is important to remember that solar and geomagnetic forcing are the most significant contributors to the TEC in the ionosphere. While the 2013 solar maximum was weak in a historical sense, during a solar maximum the induced difference in TEC can be as much as a factor of magnitude. When solar forcing is stronger, with the added variability due to sunspots, it is expected that secondary factors such as planetary waves and tides would be less significant. This may also explain why the correlation observed at NCRD was at a substantially lower altitude than the other two stations.

While stratospheric ozone and TEC variability follow a similar trend, it is apparent that day-to-day variations are not well represented. In fact, in several instances the daily stratospheric ozone concentration increases while TEC variability decreases. Other times the opposite is true. Part of this effect may be due to inaccuracies in estimating both the TEC and stratospheric ozone. Additionally, the day-to-day variability is more likely caused by primary sources of TEC variability such as the solar ionizing flux and geomagnetic activity. However, there is also the possibility that stratospheric

ozone effects on TEC variability are gradual as thermal tides in the lower stratosphere take time to amplify.

5.3 Significance of Research

This study provided evidence of the relationship between TEC variability and stratospheric ozone over a long duration and covered low-to-mid latitudes. Previous research was geared towards low latitudes and specific SSW events, which are theorized to induce a short-term increase in stratospheric ozone. This perturbation in ozone then alters the migrating tide, which has been long theorized to impact the ionosphere (Goncharenko, 2012). This research sought to examine long time-periods in order to quantify and examine the change imparted by stratospheric ozone fluctuations. By quantifying this relationship, it is not only possible to provide an estimate of TEC variability given stratospheric ozone densities, but also estimate stratospheric ozone densities using TEC variability. This effectively provides a new outlet of estimating data since knowing one parameter gives you information about the other.

The potential to approximate stratospheric ozone densities using TEC variability estimates could be particularly useful to researchers looking for additional sources of ozone data. While only a handful of models estimate stratospheric ozone concentrations, TEC estimates have much better resolution and can be derived for a vast network of receiving stations. While this research focuses primarily on thermal tides and electron density variations, ozone is an essential greenhouse gas that has the potential to exact great changes on the atmosphere and climate. Additional methods to quantify ozone would have merit in climatological research.

Using LEEDR to gauge the radiative changes resulting from a change in stratospheric ozone opens up yet another approach to quantify TEC variations. By measuring the spectral radiance for a particular day, an estimate of stratospheric ozone can be derived from ozone's IR and UV absorption bands. These bands are particularly sensitive to variations in ozone density. Path radiance can provide an estimate of stratospheric ozone, which can then be used to infer an estimate of TEC variability. In addition, given models indicate a change in the estimate of TEC variability, one can infer that there are stratospheric ozone fluctuations which are measureable in both the UV and LWIR.

The data analysis shown in this document provides evidence to the potential link between stratospheric ozone and TEC variability. While numerical evidence suggests that there is a connection between stratospheric ozone and TEC variability, there are several points that should be considered moving forward. Ozone profiles are constructed at only a handful of stations, and there is no method to collect a substantial amount of in-situ measurement above 35 km, which is the altitude in which ozonesonde balloons burst. Because of this, ozone data estimated at these levels cannot be verified. By further analyzing the latitudinal and solar cycle dependence of the relationship between stratospheric ozone and TEC variation, TEC variability models such as the GAIM can be improved upon both its short-term and long-term estimates. As such, ozone collection from other sources would help quantify this dependence.

5.4 Recommendations for Future Research

Future research into the link between stratospheric ozone concentrations and TEC variability including further evidence of a solar cycle and latitude dependence, would require the acquisition of stratospheric ozone data for new stations and times. Eventually, this information could help work towards a more accurate TEC variability model and improving the capabilities of radiative transfer models such as LEEDR. The correlation between stratospheric ozone and TEC variability should be further expanded to further explore latitudinal dependence. Including additional stations will further and more accurately quantify the stratospheric ozone and TEC variability relationship.

One of the biggest limiting factors in selecting Dobson and Brewer spectrometers as a solitary source of ozone profiles is their limited site selections. CORS data is available for a number of locations throughout the globe; however, ozone data available through Dobson and Brewer spectrometers is scarce. This is an especially difficult problem at lower latitudes. There is a Dobson spectrometer located in Hawaii; however, even though this station has total ozone records, it has no data recorded for the ozone profile. Improving current models of the TEC will require the incorporation of lesser understood drivers such as diurnal planetary tides. While the incorporation of ozone effects is a good first step in this direction, evidence shows that it does not fully cover all the secondary effects that impact TEC variability.

While Dobson and Brewer spectrometers provide the most robust ozone profile datasets, generating ozone profiles is no longer completely relegated to ground stations. There are now methods in which ozone profiles can be derived from sensors equipped on satellites. One method to access this satellite data is through Giovanni, which is an

interactive web application allowing users to utilize data without having to download it. Ozone profiles are available using the Atmospheric Infrared Sounder (AIRS), which is a spectrometer aboard the second Earth Observing System (EOS). Ozone profiles have also been available since July 2004 when the EOS Aura satellite was launched equipped with the Ozone Monitoring Instrument (OMI). This instrument retrieves ozone profiles from UV radiances in the 270 – 330 nm bandwidth. It covers 24 layers at a 2.5 km thickness per layer up to around 60 km.

The biggest question to answer in regarding satellite-based ozone profiles is whether or not they are as accurate as their ground-based counterparts. In measuring the effectiveness of satellite based instruments, the INTEX Ozonesonde Network Study (IONS-06) conducted in 2006 has proven to be a primary source. In the month of August, 424 ozonesondes were launched at 23 different sites in North America. Adding to this dataset, surface concentrations of ozone are measured at 1,188 stations across the continental United States. If ozone measurements derived from satellites were more accurate than those estimated from ground based spectrometers, it would be a simple choice to use them for analysis purposes. The reason being is that it would allow for non-site specific ozone profile sampling over the entire globe. However, satellite instruments are plagued by many of the same issues as ground based sensors. OMI consistently underestimates elevated ozone concentrations. Even after normalization, comparisons with ozonesondes reveal an upper tropospheric ozone bias of 10% (Wang et al., 2011). The total ozone measurements derived from the OMI and 27 world-wide Brewer spectrometers were compared over a 4-year period between 2005 and 2008. There was

general good agreement between the two with an overall difference of .02% and a standard deviation of 1.81 across the northern hemisphere (Bak et al., 2015).

Even if a consistent link is found between stratospheric ozone and TEC variability, currently the driving mechanism concerning modulation of the E-region wind dynamo is based more on theory than evidence. Moving forward in ionospheric forecasting will require high resolution data for this region of the ionosphere in which sampling is low. Currently, organizations like NASA are working towards defining tidal coupling and bridging the gap in this missing data. The Ionospheric Connection Explorer (ICON) is scheduled to launch in the middle of 2017 and its mission is to investigate the impact that energy and momentum from Earth's atmosphere has on the ionosphere. Additional objectives are to investigate sources of ionospheric variability, energy and momentum transfer into space, and solar and magnetospheric effects on the atmosphere space system (Immel et al., 2016). The launch was spurred by recent research highlighting an influence of the troposphere and stratosphere on regions in the boundary of space. ICON will attempt to separate the tidal components and provide evidence as to how energy and momentum from the lower atmosphere propagate into space.

The major focus of ICON will be the E-region from 110 – 180 km, which is where winds often fluctuate with altitude. ICON will further study additional secondary effects that that tides have on the ionosphere. For example, modulating the E-region dynamo produces a vertical ion drift that is measurable. Vertical ion drifts will be measured during the day and night in order to study tidal effect on electrodynamic and ionospheric forcing. It will provide wind and temperature data up to 400 km for use in the full investigation of the F-layer. A better understanding of how tides are able to change

the ionosphere is a step towards making a comprehensive model. It is clear that understanding the stratosphere's relationships with the ionosphere will be a scientific priority for the distant future.

Bibliography

Arikan, F., H. Nayir, U. Sezen, and O. Arikan (2008), "Estimation of single station interfrequency receiver bias using GPS-TEC", *Radio Sci*., 43, RS4004, doi:10.1029/2007RS003785.

Bak, J., X. Liu, J. H. Kim, K. Chance, and D. P. Haffner (2015), "Validation of OMI total ozone retrievals from the SAO ozone profile algorithm and three operational algorithms with Brewer measurements", *Atmos. Chem. Phys*., 15, 667-683, doi:10.5194/acp-15-667-2015.

Bhartia, P. K., McPeters, R. D., Flynn, L. E., Taylor, S., Kramarova, N. A., Frith, S., DeLand, M. (2013). "Solar backscatter UV (SBUV) total ozone and profile algorithm." *Atmospheric Measurement Techniques*, 6(10), 2533. doi:http://dx.doi.org/10.5194/amt-6-2533-2013

Bordi, I., Berrilli, F., and Pietropaolo, E. (2015). "Long-term response of stratospheric ozone and temperature to solar variability." *Annales Geophysicae*, 33(3), 267. doi:http://dx.doi.org/10.5194/angeo-33-267-2015

Chapman, S., and R. S. Lindzen (1970), *Atmospheric Tides: Thermal and Gravitational*, 200 pp, Gordon and Breach, New York.

Fesen, C. G., (1997) "Theoretical effects of tides and auroral activity on the low latitude ionosphere." *Journal of Atmospheric and Solar-Terrestrial Physics*, 59, 13, 1521-1532.

Fiorino, S. T., Randall, R. M., Via, M. F., Burley, J. L., (2013). "Validation of a UV-to-RF High-Spectral-Resolution Atmospheric Boundary Layer Characterization Tool." *American Meteorological Society*. doi:10.1175/JAMC-D-13-036.1

Forbes, J. M., X. Zhang, E. R. Talaat, and W. Ward (2003), "Nonmigrating diurnal tides in the thermosphere," *J. Geophys. Res*., 108, 1033, doi:10.1029/2002JA009262, A1.

Forbes, J. M., X. Zhang, S. Palo, J. Russell, C. J. Mertens, and M. Mlynczak (2008), "Tidal variability in the ionospheric dynamo region," *J. Geophys. Res*., 113, A02310, doi:10.1029/2007JA012737.

Friedman, J. S., X. Zhang, X. Chu, and J. M. Forbes (2009), "Longitude variations of the solar semidiurnal tides in the mesosphere and lower thermosphere at low latitudes observed from ground and space," *J. Geophys. Res*., 114, D11114, doi:10.1029/2009JD011763.

Fritts, D.C., Abdu, M.A., Batista, B.R. et al. (2009). "The spread F Experiment (SpreadFEx): Program overview and first results." *Earth Planet Sp* 61: 411. doi:10.1186/BF03353158

Gong, Y., Q. Zhou, and S. Zhang (2013), "Atmospheric tides in the low-latitude E and F regions and their responses to a sudden stratospheric warming event in January 2010," *J. Geophys. Res. Space Physics*, 118, 7913–7927, doi:10.1002/2013JA019248.

Gonsharenko, L. P., Chau, J. L., Coster, A. J. (2010) "Unexpected connections between the stratosphere and ionosphere." *Geophysical Research Letters*, 37. doi:10.1029/2010GL043125-2010

Gonsharenko, L. P., Coster, A. J., Chau, J. L., Valladares, C. E. (2010) "Impact of sudden stratospheric warmings on equatorial ionization anomaly." *Journal of Geophysical*, 115. doi:10.1029/2010JA015400-2010

Gonsharenko, L. P., Coster, A. J., Plumb, R. A., Domeisen, D. I. V. (2012). "The potential role of stratospheric ozone in the stratosphere-ionosphere coupling during stratospheric warmings." *Geophysical Research Letters*, 39. doi:10.1029/2012GL051261-2012

Hagan, M. E., and J. M. Forbes (2003), "Migrating and non-migrating semidiurnal tides in the upper atmosphere excited by tropospheric latent heat release," *J. Geophys. Res*., 108, 1062, doi:10.1029/2002JA009466, A2.

Jones, M. Jr., Forbes, J. M., Hagan, M. E., Maute, A., (2014) "Impacts of vertically propagating tides on the mean state of the ionosphere-thermosphere system." *Journal of Geophysical Research: Space Physics*, 119, 2197-2213 doic10.102/2013JA019744.

Immel, T.J., and England, S. L., Mendel, Hellis, R. A., Englet, C. R., Edelstein, J., Frey H. U., Taylor, E. R., Craig, W. W., Bust, G., Crowley, G., Forbes, J. M., Gerard, J. C., Harlander, J., Huba, J. D., Bubert, B., Kamalabadi, F., Makela, J. J., Maute, A. I., Meier, R. R., Raftery C., Rochus P., Siegmund O. H. W., Stepahn A. W., Swenson, G. R., Frey, S., Hysell, D., Saito, A., (2016). "The Ionospheric Connection Explorer Mission." *Berkeley,* Doi:http://icon.ssl.berkeley.edu/Portals/devIcon/GeneralDocuments/ICON_Mission_Goals_and_Design_July2016_DRAFT.pdf?ver=2016-07-26-172604-203

Korenkov, Y. N., Klimenko, V. V., Klimenko, M. V., Bessarab, F. S., Korenkova, N. A., Ratovsky, K. G., Condor, P. (2012). "The global thermospheric and ionospheric response to the 2008 minor sudden stratospheric warming event." *Journal of Geophysical Research.Space Physics*, 117(10) doi:http://dx.doi.org/10.1029/2012JA018018

Kratz, D. P., Cess, R. D. (1988). "Infrared Radiation Models for Atmospheric Ozone." *Journal of Geophysical Research* 93, 7047-7054.

Lal, M. (2001) "A model study of the atmospheric heating rates due to O3, H2O and O2." *Indian Journal of Radio & Space Physics* 30, 254-259.

Laštovička, J. (2006) "Forcing of the ionosphere by waves from below." *Journal of Atmospheric and Solar-Terrestrial Physics* 68, 479-497.

Lawrence, B. N. and Randel, W. J. (1996) Variability in the mesosphere observed by the Nimbus 6 pressure modulator radiometer, J. Geophys. Res., 101, 23 475–23 489.

Middlebrook, A. M., Tolbert, M. A. (2000). "Stratospheric Ozone Depletion." *University Science Books* https://www.ucar.edu/communications/gcip/m1sod/m1pdf.pdf

Mukhtarov, P., D. Pancheva, B. Andonov, and L. Pashova (2013), "Global TEC maps based on GNSS data: 1. Empirical background TEC model," *J. Geophys. Res. Space Physics*, 118, 4594–4608, doi:10.1002/jgra.50413.

Oberheide, J., M. E. Hagan, R. G. Roble, and D. Offermann (2002), "Sources of nonmigrating tides in the tropical middle atmosphere," *J. Geophys. Res.*, 107(D21), 4567, doi:10.1029/2002JD002220, 2002.

Oberheide, J., Shiokawa, K., Gurubaran, S. et al. (2015). "Prog. in Earth and Planet." *Sci*. (2015) 2: 2. doi:10.1186/s40645-014-0031-4

Pedatella, N. M., and H.–L. Liu (2013), "The influence of atmospheric tide and planetary wave variability during sudden stratosphere warmings on the low latitude ionosphere," *J. Geophys. Res. Space Physics*, 118, 5333–5347 doi:10.1002/jgra.50492.

Pancheva, D., and Mukhtarov, P. (2012). "Global Response of the Ionosphere to Atmospheric Tides Forced from Below: Recent Progress Based on Satellite Measurements." *Space Science Reviews*, 168(1-4), 175-209. doi:10.1007/s11214-011-9837-1

Pancheva, D., P. Mukhtarov, and A. K. Smith, (2013): "Climatology of the migrating terdiurnal tide (TW3) in SABER/TIMED temperatures." *Journal of Geophysical Research-Space Physics*, 118, 1755-1767, doi:10.1002/jgra.50207.

Pancheva, D., P. Mukhtarov, and A. K. Smith, (2014): "Non-migrating tidal variability in the SABER/TIMED mesospheric ozone." *Geophys. Res. Lett*., 41, 4059–4067, doi:10.1002/2014GL059844.

Petropavlovskikh, I., P. K. Bhartia, and J. DeLuisi (2005), "New Umkehr ozone profile retrieval algorithm optimized for climatological studies," *Geophys. Res. Lett*., 32, L16808, doi:10.1029/2005GL023323.

Petropavlovskikh, I., Evans, R., McConville, G., Oltmans, S., Quincy, D., Lantz, K., and Flynn, L. (2011). "Sensitivity of Dobson and Brewer Umkehr ozone profile retrievals to ozone cross-sections and stray light effects." *Atmospheric Measurement Techniques, 4*(9), 1841-1853

Randel W, J. (1993) "Global variations of zonal mean ozone during stratospheric warming events." *Journal of the Atmospheric Sciences*, 50 (3308–3321) (1993), p. 1993

Rishbeth, H. (2006). "F-region links with the lower atmosphere?" *Journal of ATMOSPHERIC AND SOLAR-TERRESTRIAL PHYSICS*. 68. 469-478.

Schunk, R. W., Gardner, L., Scherliess, L., and Zhu, L. (2012). "Problems associated with uncertain parameters and missing physics for long-term ionosphere-thermosphere forecasting." *Radio Science, 47* doi:http://dx.doi.org/10.1029/2011RS004911

Sezen, U., F. Arikan, O. Arikan, O. Ugurlu, and A. Sadeghimorad (2013), "Online, automatic, near-real time estimation of GPS-TEC: IONOLAB-TEC," *SpaceWeather*, *11*, 297–305, doi:10.1002/swe.20054.

E. P. Shettle and R. W. Fenn (1979), “Models for the aerosols of the lower atmosphere and the effects of humidity variations on their optical properties,” Rep. AFGL-TR-79-0214, *Air Force Geophysics Lab*., Hanscom, MA

Sridharan, S., et al. (2012), “Variabilities of mesospheric tides during sudden stratospheric warming events of 2006 and 2009 and their relationship with ozone and water vapour,*” J. Atmos. Sol. Terr. Phys*., 78–79, 108–115, ISSN 1364–6826, doi:10.1016/j.jastp.2011.03.013.

Stolarski, R., Bojkov, R., Bishop, L., Zerefos, C., Staehelin, J., and Zawodny, J. (1992). Measured trends in stratospheric ozone. *Science (Washington, D.C.); (United States), 256:5055*(5055). doi:10.1126/science.256.5055.342

University of Connecticut (2015). Critical Values of the Pearson Product-Moment Correlation Coefficient [Table]. r Critical Value Table. Retrieved on 2016.12.05 from http://researchbasics.education.uconn.edu/r_critical_value_table/

Wang, L., Newchurch, M. J., Biazar, A., Liu, X., Kuang, S., Khan, M., and Chance, K. (2011). “Evaluating AURA/OMI ozone profiles using ozonesonde data and EPA surface measurements for August 2006,” *Atmos. Environ.,* 45, 5523–5530., doi:10.1016/j.atmosenv.2011.06.012, 2011.

Whiteman, C. D., and X. Bian, (1996). “Solar semidiurnal tides in the troposphere: Detection by radar profiles.” *Bull. Amer. Meteor. Soc*., 77, 529–542.

REPORT DOCUMENTATION PAGE

Form Approved
OMB No. 074-0188

1. REPORT DATE *(DD-MM-YYYY)*	2. REPORT TYPE	3. DATES COVERED *(From – To)*
10-03-2017	Master's Thesis	June 2015 – March 2017

TITLE AND SUBTITLE

Total electron count variability and stratospheric ozone effects on solar backscatter and LWIR emissions

5a. CONTRACT NUMBER

5b. GRANT NUMBER

5c. PROGRAM ELEMENT NUMBER

6. AUTHOR(S)

Ross, John S., Captain, USAF

5d. PROJECT NUMBER

5e. TASK NUMBER

5f. WORK UNIT NUMBER

7. PERFORMING ORGANIZATION NAMES(S) AND ADDRESS(S)

Air Force Institute of Technology
Graduate School of Engineering and Management (AFIT/ENP)
2950 Hobson Way, Building 640
WPAFB OH 45433-8865

8. PERFORMING ORGANIZATION REPORT NUMBER

AFIT-ENP-MS-17-M-103

9. SPONSORING/MONITORING AGENCY NAME(S) AND ADDRESS(ES)

A National Program Office

10. SPONSOR/MONITOR'S ACRONYM(S)

AF/A3W

AFRL/RHIQ (example)

11. SPONSOR/MONITOR'S REPORT NUMBER(S)

12. DISTRIBUTION/AVAILABILITY STATEMENT

DISTRUBTION STATEMENT A. APPROVED FOR PUBLIC RELEASE; DISTRIBUTION UNLIMITED.

13. SUPPLEMENTARY NOTES

14. ABSTRACT

The development of an accurate ionospheric Total Electron Content (TEC) model is of critical importance to High Frequency (HF) radio wave propagation. However, the TEC is highly variable and is continuously influenced by geomagnetic storms, extreme Ultraviolet (UV) radiation, diurnal variation, and planetary waves. The ability to capture this variability is essential to improve current TEC models. Analysis of the growing body of data involving ionospheric fluctuations and thermal tides has revealed persistent correlation between increases in stratospheric ozone and variability of the TEC. The spectral properties of ozone show that it is a greenhouse gas that alters longwave emissions from Earth and interacts with the UV spectrum coming from the sun. This study uses the Laser Environment Effects Definition and Reference (LEEDR) to model and simulate the effect of changes in stratospheric ozone on solar backscatter and longwave terrestrial emissions and infer TEC variability.

15. SUBJECT TERMS

Total Electron Content, Thermal Tides, Ozone, Infrared, Ultraviolet, Emissions, Backscatter

16. SECURITY CLASSIFICATION OF:			17. LIMITATION OF ABSTRACT	18. NUMBER OF PAGES	19a. NAME OF RESPONSIBLE PERSON
a. REPORT	b. ABSTRACT	c. THIS PAGE			Dr. Steven Fiorino, AFIT/ENP
U	U	U	UU	93	19b. TELEPHONE NUMBER *(Include area code)* (910) 584-1891, (NOT DSN) (john.ross@afit.edu)

Standard Form 298 (Rev. 8-98)
Prescribed by ANSI Std. Z39-18